iScience

CellPress
OPEN ACCESS

Article

ADAMTS18 Deficiency Leads to Pulmonary Hypoplasia and Bronchial Microfibril Accumulation

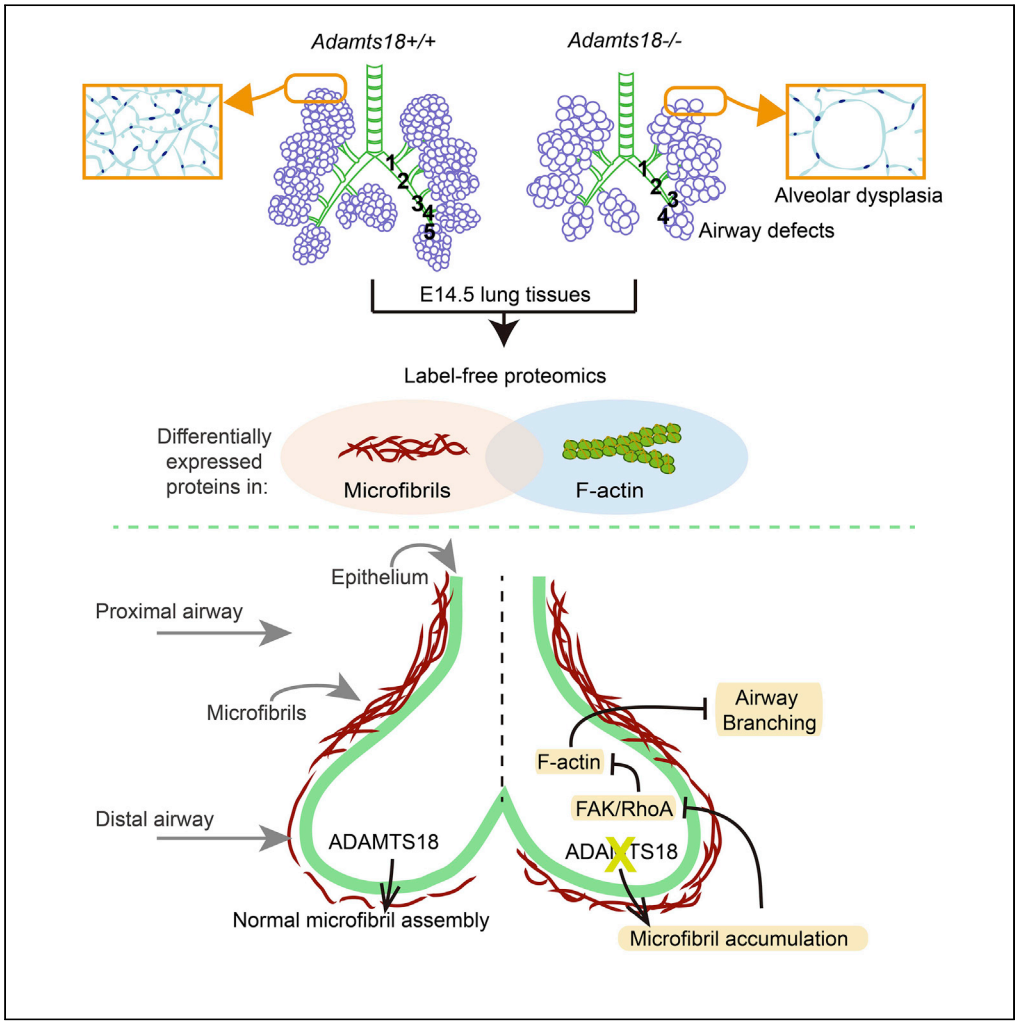

Tiantian Lu, Xiaotian Lin, Yi-Hsuan Pan, ..., Bi-Sen Ding, Suying Dang, Wei Zhang

suyingdang@shsmu.edu.cn (S.D.)
wzhang@sat.ecnu.edu.cn (W.Z.)

HIGHLIGHTS

ADAMTS18 serves as a morphogen in early lung development

ADAMTS18 deficiency increases lung susceptibility to injuries

ADAMTS18 affects airway branching by regulating bronchial microfibril abundance

Lu et al., iScience *23*, 101472
September 25, 2020
https://doi.org/10.1016/j.isci.2020.101472

iScience

CellPress
OPEN ACCESS

Article

ADAMTS18 Deficiency Leads to Pulmonary Hypoplasia and Bronchial Microfibril Accumulation

Tiantian Lu,[1] Xiaotian Lin,[1] Yi-Hsuan Pan,[1] Ning Yang,[1] Shuai Ye,[1] Qi Zhang,[1] Caiyun Wang,[1] Rui Zhu,[1] Tianhao Zhang,[1] Thomas M. Wisniewski,[2] Zhongwei Cao,[3] Bi-Sen Ding,[3] Suying Dang,[4,*] and Wei Zhang[1,5,*]

SUMMARY

ADAMTSs (a disintegrin and metalloproteinase with thrombospondin motifs) are secreted metalloproteinases that play a major role in the assembly and degradation of the extracellular matrix (ECM). In this study, we show that ADAMTS18, produced by the epithelial cells of distal airways and mesenchymal cells in lung apex at early embryonic stages, serves as a morphogen in lung development. ADAMTS18 deficiency leads to reduced number and length of bronchi, tipped lung apexes, and dilated alveoli. These developmental defects worsen lipopolysaccharide-induced acute lung injury and bleomycin-induced lung fibrosis in adult *Adamts18*-deficient mice. ADAMTS18 deficiency also causes increased levels of fibrillin1 and fibrillin2, bronchial microfibril accumulation, decreased focal adhesion kinase signaling, and disruption of F-actin organization. Our findings indicate that ECM homeostasis mediated by ADAMTS18 is pivotal in airway branching morphogenesis.

INTRODUCTION

The lungs provide two vital physiological functions including passive gas exchange (alveolar respiration) and innate immune defense against microbial infections. Early lung development has a lifelong effect on respiratory health and disease (Stocks et al., 2013). Factors that adversely affect lung development may accelerate lung function decline and worsen respiratory morbidity in adulthood. Therefore, identification of key cellular and molecular mechanisms involved in early lung development is important for the development of novel strategies to prevent lung diseases.

ADAMTSs (a disintegrin and metalloproteinase with thrombospondin motifs) are a group of 19 secreted metalloproteinases with major roles in the assembly and degradation of the extracellular matrix (ECM). Previous studies have shown that some of these enzymes are produced by lung cells and are involved in lung pathophysiology. Among them, ADAMTS1 is secreted by developing lung epithelial cells at embryonic stages (Thai and Iruela-Arispe, 2002). *Adamts9* mRNAs are expressed in interstitial cells at E14.5 (Jungers et al., 2005). *Adamts10* mRNAs are present in the cells surrounding the bronchial tree and blood vessels at E14.5 to E17.5 (Somerville et al., 2004). ADAMTS1, 4, 9, 12, and 15 have been implicated in asthma (Di Valentin et al., 2009; Kurz et al., 2006; Paulissen et al., 2006).

In humans, ADAMTS18 mutations have been linked to tumorigenesis (Jin et al., 2007), developmental eye disorders (Aldahmesh et al., 2011, 2013; Peluso et al., 2013), reduced bone mineral density (Xiong et al., 2009), and decreased white matter integrity of the brain (Lopez et al., 2012). To further study the role of ADAMTS18 *in vivo*, we developed an *Adamts18* knockout (*Adamts18*$^{-/-}$) mouse strain (Lu et al., 2017) and found that *Adamts18*$^{-/-}$ mice exhibited severely dilated alveoli. This novel finding prompted further studies on the role of ADAMTS18 in lung pathophysiology.

In this study, we demonstrated that *Adamts18* is spatiotemporally expressed in the branching epithelium of distal airways and mesenchymal cells in lung apex at early development stages. We also found that ADAMTS18 deficiency leads to reduced number and length of bronchi, tipped lung apex, dilated alveoli, and increased susceptibility to lung injuries. In addition, ADAMTS18 was found to affect bronchus branching partly by interacting with fibrillin1 (FBN1) and regulating the abundance of microfibrils.

[1]Key Laboratory of Brain Functional Genomics (Ministry of Education and Shanghai), School of Life Sciences, East China Normal University, 3663 North Zhongshan Road, Shanghai 200062, China

[2]Departments of Neurology, Pathology and Psychiatry, New York University School of Medicine, New York, NY 10016, USA

[3]Key Laboratory of Birth Defects and Related Diseases of Women and Children of MOE, State Key Laboratory of Biotherapy, West China Second University Hospital, Sichuan University, and Collaborative Innovation Center for Biotherapy, Chengdu, China

[4]Department of Biochemistry and Molecular Cell Biology, Shanghai Jiao Tong University School of Medicine, 227 South Chongqing Road, Shanghai 200025, China

[5]Lead Contact

*Correspondence: suyingdang@shsmu.edu.cn (S.D.), wzhang@sat.ecnu.edu.cn (W.Z.)

https://doi.org/10.1016/j.isci.2020.101472

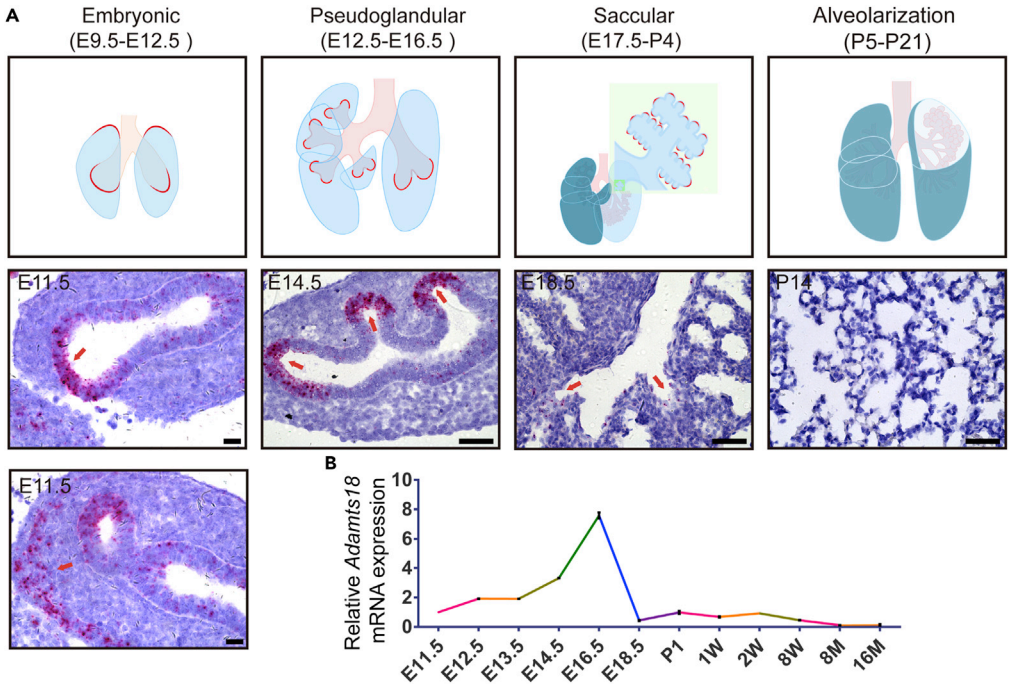

Figure 1. Spatiotemporal Expression of Adamts18 mRNAs in Mouse Lungs

(A) Upper panels: Cartoon picture illustrates the spatiotemporal expression pattern of *Adamts18* mRNAs at different stages of lung development in mice. Lower panels: *In situ* hybridization (ISH) of *Adamts18* mRNA in wild-type mouse lungs (consecutive transverse sections of lung tissue). ISH-positive signals are shown as pink dots in cells (red arrows). Scale bar, 50 μm.

(B) qRT-PCR analysis of *Adamts18* mRNA from E11.5 to 16-month-old mouse lungs (n = 3/time point). The relative quantity of *Adamts18* mRNA was normalized to that of the housekeeping gene *Gapdh* using the $\Delta\Delta Ct$ method. Data are expressed as mean ± SEM.

See also Table S5.

RESULTS

Expression of Adamts18 in Mouse Lungs

To investigate the role of ADAMTS18 in lung development, *Adamts18* mRNA distribution at different developmental stages was determined by *in situ* hybridization. In embryonic lungs (E9.5–E12.5), *Adamts18* mRNAs were detected in the epithelium of branching tips and mesenchymal cells in lung apex. At pseudoglandular stage (E12.5–E16.5), *Adamts18* mRNAs were most abundant in distal epithelium. At saccular stage (E17.5–P4), the levels of *Adamts18* mRNAs were very low in the epithelium of the distal part of bronchiole. At alveolarization stage (P5–P21), *Adamts18* mRNAs were barely detectable in both airway and alveolar cells (Figure 1A). Determination of *Adamts18* mRNA levels by quantitative RT-PCR (qRT-PCR) in lung tissues from E11.5 to 16-month-old mice demonstrated that *Adamts18* is a phase-specific gene and is expressed only in the early embryonic stages (Figure 1B).

Decreased Number and Length of Bronchi due to ADAMTS18 Deficiency

At E14.5, the lung apexes of *Adamts18*$^{-/-}$ mice were bilaterally tipped, whereas those of *Adamts18*$^{+/+}$ mice had a smooth contour (Figure 2A). To characterize branching morphogenesis, E11.5 lungs of both *Adamts18*$^{+/+}$ and *Adamts18*$^{-/-}$ mice were *in vitro* cultured and examined every 24 h for 72 h (Figure 2B). No macroscopic differences between the two groups of lung explants were observed at the time of dissection. At 24 h of culture, *Adamts18*$^{-/-}$ lungs exhibited an abnormal branching pattern at the distal part of the right lung. At 48 and 72 h of culture, the number of branches in *Adamts18*$^{-/-}$ lungs was significantly decreased compared with that of *Adamts18*$^{+/+}$ lungs (48 h, 35.5 ± 0.5 versus 25 ± 2.9, p = 0.031; 72 h, 56.5 ± 2.5 versus 41 ± 1.6, p = 0.007) (Figure 2C). In addition, the lengths of R5 and R2 secondary bronchi (Figure 2D) in cultured *Adamts18*$^{-/-}$ lung explants were significantly shorter than those of *Adamts18*$^{+/+}$ lung explants (R5, 7.07 ± 0.14 mm versus 4.41 ± 0.61 mm, p = 0.018; R2, 5.61 ± 0.06 mm versus 3.94 ±

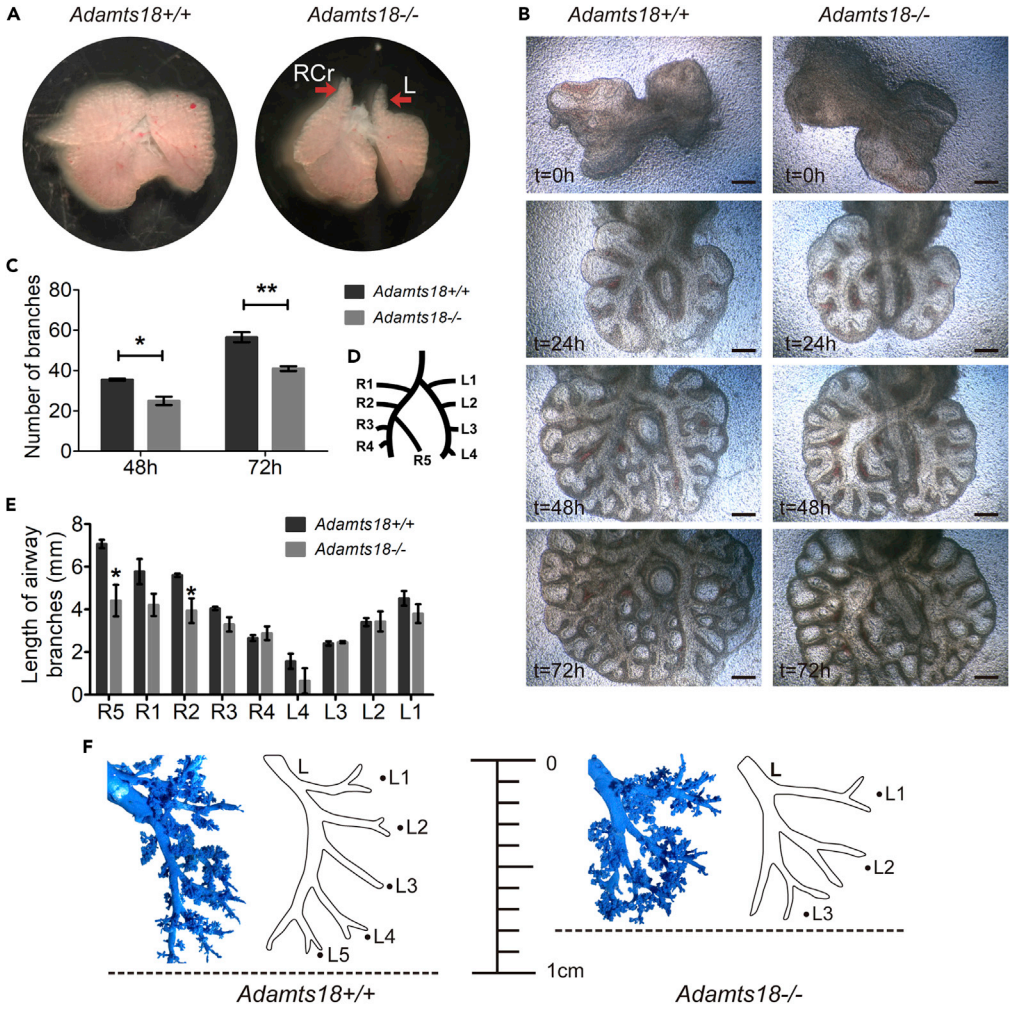

Figure 2. Bronchial Tree in Mouse Lungs

(A) Representative images of embryonic lungs at E14.5. Red arrows indicate tipped apexes of *Adamts18*$^{-/-}$ lungs.

(B) E11.5 lungs were cultured *in vitro* and photographed at different time points (0–72 h). Scale bar, 200 μm.

(C) Branch number of each explant at 48 and 72 h of culture.

(D) Cartoon illustration of bronchial branches in lungs. L1-L4 and R1-R5 represent bronchial branches in left and right lungs, respectively.

(E) Lengths of L1-L4 and R1-R5 at 48 h of culture. Scale bar, 50 μm.

(F) Left lobe lung cast of 12-week-old *Adamts18*$^{+/+}$ and *Adamts18*$^{-/-}$ mice.

Results in (C and E) are expressed as mean ± SD. (n = 4; *p < 0.05; **p < 0.01; Student's t test). These experiments were repeated independently at least three times. RCr, right cranial; L, left.

See also Figures S2 and S5.

0.47 mm, p = 0.031) (Figure 2E), suggesting a role of ADAMTS18 in epithelial mobility. At 12 weeks old, left lung airway casting showed a decreased bronchus number in *Adamts18*$^{-/-}$ mice compared with *Adamts18*$^{+/+}$ controls. The length from apical to the bottom was shorter in *Adamts18*$^{-/-}$ lungs than in normal *Adamts18*$^{+/+}$ lungs (Figure 2F).

Abnormal Lung Morphology in *Adamts18*$^{-/-}$ Mice

Adult *Adamts18*$^{-/-}$ lungs exhibited several morphologic features that are different from those of *Adamts18*$^{+/+}$ lungs, including tipped distal part, bulged center part in the ventral side of left lobes, and shorter axis length (Figure 3A). There was no significant difference in the ratio of lung weight to body weight between *Adamts18*$^{-/-}$ and *Adamts18*$^{+/+}$ mice (Figure 3B). Histological analyses of lungs showed linear atelectasis at postnatal day 1 and dilated alveoli with decreased number of radical alveolar counts

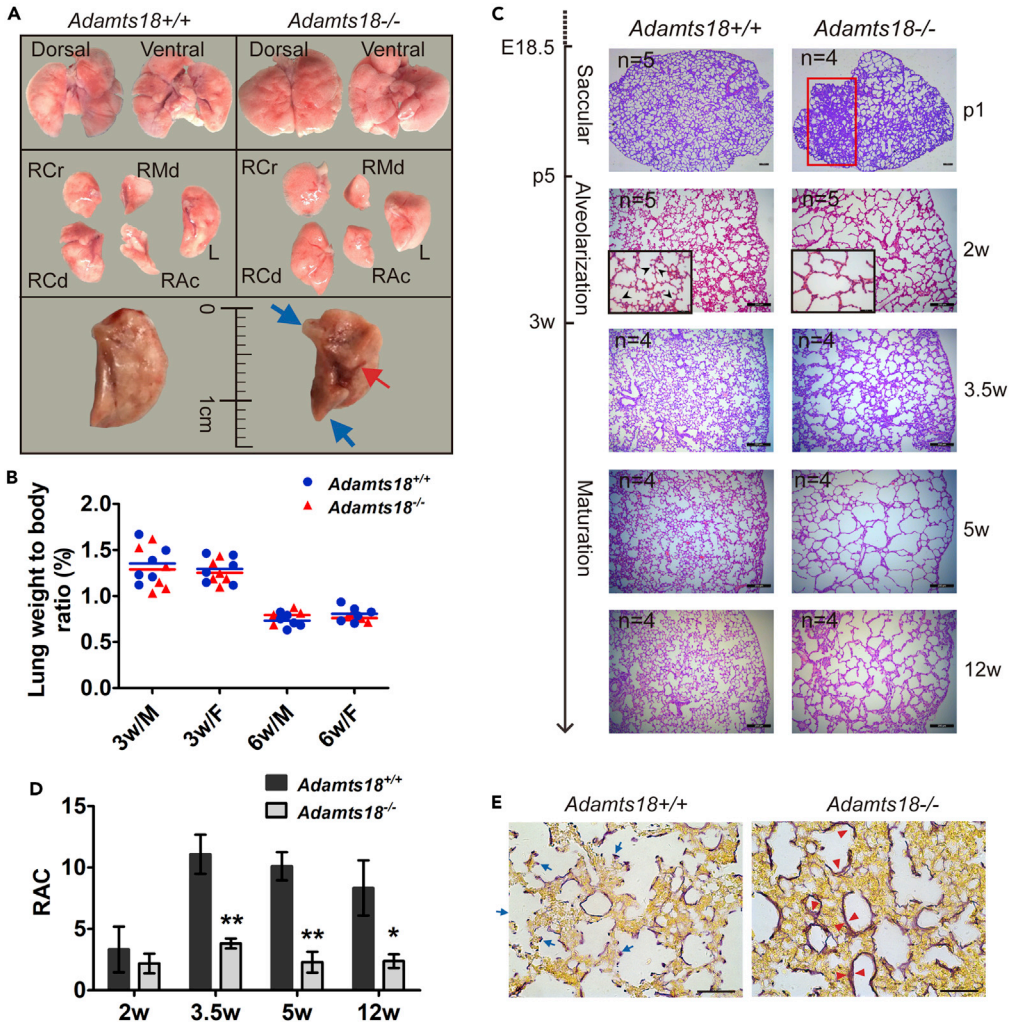

Figure 3. Abnormal Lung Morphogenesis in *Adamts18*$^{-/-}$ Mice

(A) Gross morphology of 12-week-old adult lungs. Dorsal and ventral views are displayed in upper panels. Separated right cranial (RCr), right middle (RMd), right accessory (RAc), right caudal (RCd), and left (L) lobes are shown in middle panels. In lower panels, blue arrows indicate tipped distal parts of the left lobe in *Adamts18*$^{-/-}$ mice. Red arrow denotes a ventral central bulge.

(B) Lung weight to body weight ratio (%) at 3 and 6 weeks (w). M, male; F, female. Each dot or triangle represents one individual; data means are shown by solid horizontal lines.

(C) Representative images of hematoxylin and eosin (H&E)-stained lung sections of *Adamts18*$^{+/+}$ and *Adamts18*$^{-/-}$ mice at indicated development stages. Red box indicates an area with linear atelectasis in *Adamts18*$^{-/-}$ lung at postnatal day 1 (p1). Black arrowheads in boxed area indicate sprouting secondary crests in *Adamts18*$^{+/+}$ lungs. Scale bar, 200 μm.

(D) Quantification of radial alveolar count (RAC). Results are expressed as mean ± SD (n = 4 or 5/group; *$p < 0.05$; **$p < 0.01$; Student's t test).

(E) Representative Hart's staining of lung elastin fibers in 2-week-old mice. Blue arrows indicate thin elastin distribution in secondary crests and on alveolar walls in *Adamts18*$^{+/+}$ mice. Red arrowheads indicate thicker elastin deposition on alveolar walls in *Adamts18*$^{-/-}$ mice. Scale bar, 50 μm.

See also Figure S1 and Table S1.

(RACs) in *Adamts18*$^{-/-}$ mice after alveolar maturation (Figures 3C and 3D). Elastin and collagen are the two main ECM proteins during alveolar septation. With Hart's staining, a thicker elastin layer was observed on the alveolar walls of 2-week-old *Adamts18*$^{-/-}$ mice compared with their *Adamts18*$^{+/+}$ littermates (Figure 3E). Determination of mRNA levels by qRT-PCR of key proteins involved in elastic fiber synthesis, assembly, and degradation revealed that only the expression of *Tropoelastin* and elastin degradation protease *Mmp2* was significantly increased in *Adamts18*$^{-/-}$ lungs; no significant change in the expression of

other molecules was observed (Figure S1A). In addition, lung collagen of the two genotypes of mice showed no significant difference at mRNA levels by qRT-PCR (Figure S1B) and protein levels by Sirius red staining (Figure S1C).

Increased Susceptibility to LPS-Induced Acute Lung Injury and Bleomycin-Induced Lung Fibrosis due to ADAMTS18 Deficiency

There were no differences in basic lung functions between *Adamts18*$^{+/+}$ and *Adamts18*$^{-/-}$ mice (Table S1). However, *Adamts18*$^{-/-}$ mice (8 weeks old) showed more severe pathological injury (e.g., inflammation and bleeding) with a higher pathological score than *Adamts18*$^{+/+}$ littermates (8 weeks old) after intraperitoneal injection of lipopolysaccharide (LPS) (Figures 4A and 4B). Bronchoalveolar lavage fluid (BALF) cell counts were significantly increased 24 h after LPS injection in both genotypes of mice compared with saline-injected control mice (Figure 4C). However, *Adamts18*$^{-/-}$ lungs had a higher percentage of polymorphonuclear neutrophil (PMN) in BALF than *Adamts18*$^{+/+}$ lungs (Figure 4D). *Adamts18*$^{-/-}$ lungs also showed a significant increase in CD11b^{+} neutrophil infiltration and interleukin (IL)-6 expression in injured lung tissues (Figures 4E and 4F). The release of neutrophil extracellular traps (NETs) was barely detectable in both genotypes of mice (Figure 4G).

Adamts18$^{-/-}$ mice also exhibited a higher mortality rate than *Adamts18*$^{+/+}$ mice (Figure 5A) and more severe lung inflammation and fibrosis after intratracheal injection of bleomycin (Figures 5B–5D). To determine whether LPS or bleomycin induced *Adamts18* expression, *Adamts18* mRNAs levels in the lungs of LPS- or bleomycin-treated *Adamts18*$^{+/+}$ mice were measured by qRT-PCR. Results showed that LPS or bleomycin treatment did not result in increased transcription of *Adamts18* mRNAs in the lungs of these mice at various time points after the treatment (Figures 4H and 5E).

Branching-Related Signaling Molecules in *Adamts18*$^{-/-}$ Lungs

Airway branching is controlled by growth factors and matrix proteins in the epithelium and mesenchyme (Stocks et al., 2013). To determine whether the aberrant bronchus structure in *Adamts18*$^{-/-}$ lungs is related to altered expressions of these factors, mRNA levels of several critical signaling transducers were determined at E14.5. The mRNA levels of *Fgf10*, *Wnt2*, and *Bmp4* in lung tissues were similar between the two genotypes of mice. However, mRNA levels of *Fgfr2* and *Shh* were significantly increased in *Adamts18*$^{-/-}$ lungs compared with *Adamts18*$^{+/+}$ lungs (Figure S2A). *Hhip* and *Ptch1* genes are direct targets of SHH signaling (Kugler et al., 2015), and Ext1 has been shown to control SHH-FGF10 signaling (He et al., 2017). Results showed that mRNA levels of *Hhip*, *Ptch1*, and *Ext1* were comparable between *Adamts18*$^{-/-}$ and *Adamts18*$^{+/+}$ lungs (Figure S2B). Immunohistochemistry (IHC) analysis of the distribution of FGF10 and FGFR2 in E14.5 lungs also showed no significant difference between the two genotypes of mice (Figure S2C).

Embryonic Lung Proteomes

To investigate the role of ADAMTS18 in embryonic bronchus branching, proteins in E14.5 lungs from *Adamts18*$^{-/-}$ and *Adamts18*$^{+/+}$ mice were analyzed by label-free mass spectrometry. A total of 5,797 proteins were identified (data not show). The abundance of 203 lung proteins (3.5%) was significantly different between *Adamts18*$^{-/-}$ and *Adamts18*$^{+/+}$ lungs. Gene ontology term and pathway analyses of significantly changed proteins by Metascape revealed enrichment of proteins of several pathways related to ribosome, supramolecular fiber organization, and protein folding (Figures S3A and S3B). Forty-three proteins were enriched in the category of supramolecular fiber organization, suggesting disarrangements in actin fiber and ECM (Table S2). Among them, the abundance of two major components of microfibrils, fibrillin1 (FBN1) and FBN2, was increased in *Adamts18*$^{-/-}$ lungs.

Increased Levels of FBN1 and FBN2 and Accumulation of Microfibrils in *Adamts18*$^{-/-}$ Bronchi

Precise spatiotemporal regulation of ECM proteins is essential for lung development (Zhou et al., 2018). Western blotting confirmed that the levels of FBN1 and FBN2 were significantly higher in *Adamts18*$^{-/-}$ mice than in *Adamts18*$^{+/+}$ mice (Figure 6A). FBN1 and FBN2 proteins were barely detectable in the distal airway of E14.5 *Adamts18*$^{+/+}$ mice by immunofluorescence staining. However, deposition of FBN1 and FBN2 was seen around the distal airway epithelium of E14.5 *Adamts18*$^{-/-}$ lungs (Figure 6B). These two fibrillin proteins were also found in the proximal airway, but there was no significant difference in their abundance in *Adamts18*$^{+/+}$ and *Adamts18*$^{-/-}$ lungs (Figure S4). Transmission electron microscopic images

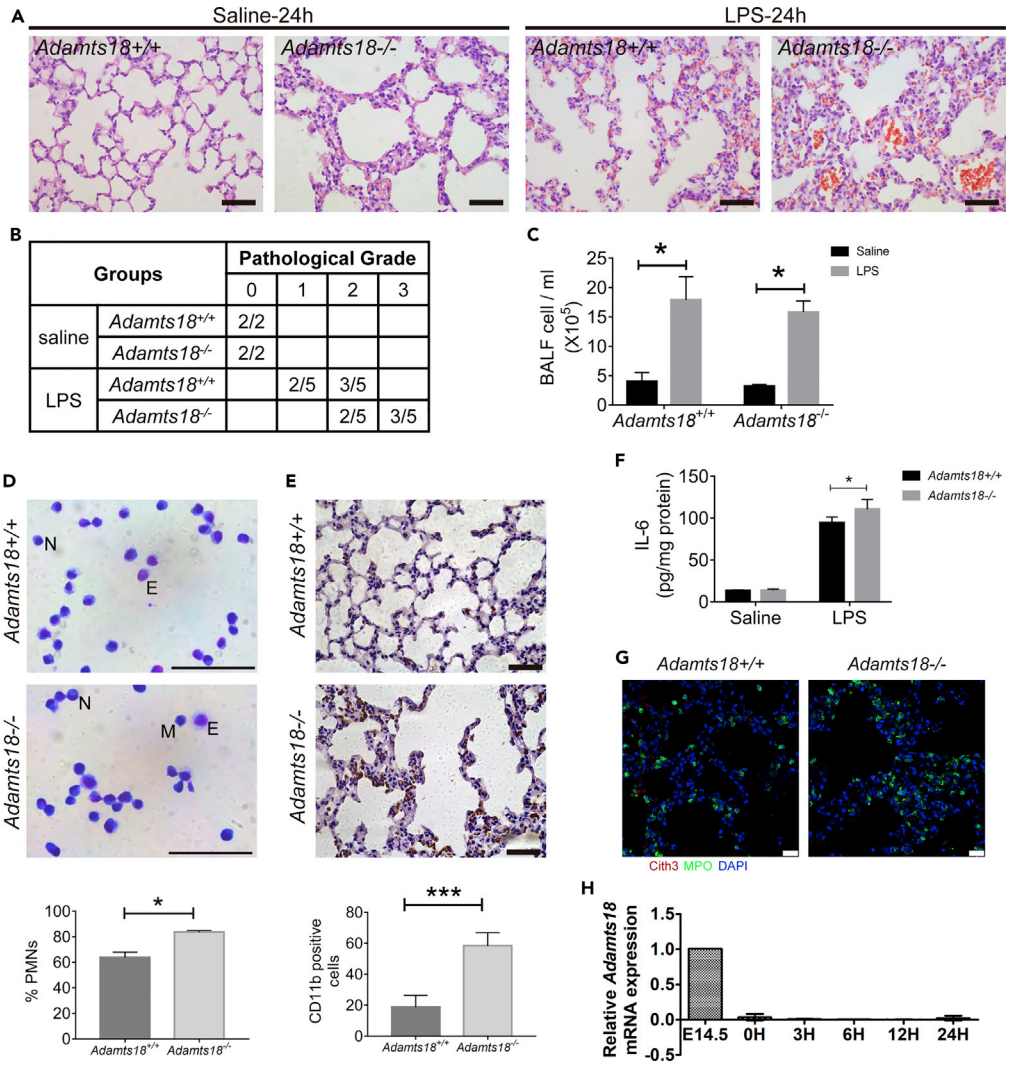

Figure 4. Increased Susceptibility of *Adamts18*$^{-/-}$ Mice to Lipopolysaccharide (LPS)-Induced Acute Lung Injury

(A) Representative images of H&E-stained lung sections of saline-treated (left panels) or LPS-treated (right panels) mice. Scale bar, 50 μm.

(B) Pathological grade of lung injury (n = 5/group).

(C) Total number of cells in bronchoalveolar lavage fluid (BALF) collected 24 h after LPS treatment. Results are expressed as mean ± SD (n = 3/group, *p < 0.05, Student's t test).

(D) Diff-quick staining of BALF cells for quantification of neutrophils (% polymorphonuclear neutrophil). N, neutrophil, E, eosinophil, M, monocyte. Scale bar, 50 μm. Results are expressed as mean ± SD (n = 3/group, *p < 0.05, Student's t test).

(E) Immunostaining of CD11b^{+} neutrophils in lung sections of LPS-treated mice. Quantification of CD11b^{+} cells in each microscopic field was performed with ImageJ. Each lung section was analyzed for 5 fields. Results are expressed as mean ± SD (N = 5/group, ***p < 0.001, Student's t test). Scale bar, 50 μm.

(F) IL-6 expression in lung tissues of saline- or LPS-treated mice was analyzed by ELISA. Results are expressed as mean ± SD (n = 5/group, *p < 0.05, Student's t test).

(G) Confocal microscopy of Cit-H3^{+}MPO^{+} neutrophil extracellular traps (NETs) in mouse lung sections. Scale bar, 100 μm.

(H) Relative mRNA levels of *Adamts18* at different time points of LPS-treated *Adamts18*$^{+/+}$ mice determined by quantitative real-time RT-PCR (n = 3/time point). The quantity of *Adamts18* mRNA was normalized to that of the housekeeping gene *Gapdh* using the *ΔΔCt* method. Data are expressed as mean ± SEM.

See also Table S4.

showed that *Adamts18*$^{-/-}$ lungs had a thicker layer of microfibrils in the basement membrane surrounding epithelial tubes (Figure 6C). Results of qRT-PCR analysis showed that *Fbn2* mRNA levels were 1.4-fold higher in *Adamts18*$^{-/-}$ lungs than in *Adamts18*$^{+/+}$ lungs, whereas *Fbn1* mRNA levels in *Adamts18*$^{-/-}$ lungs

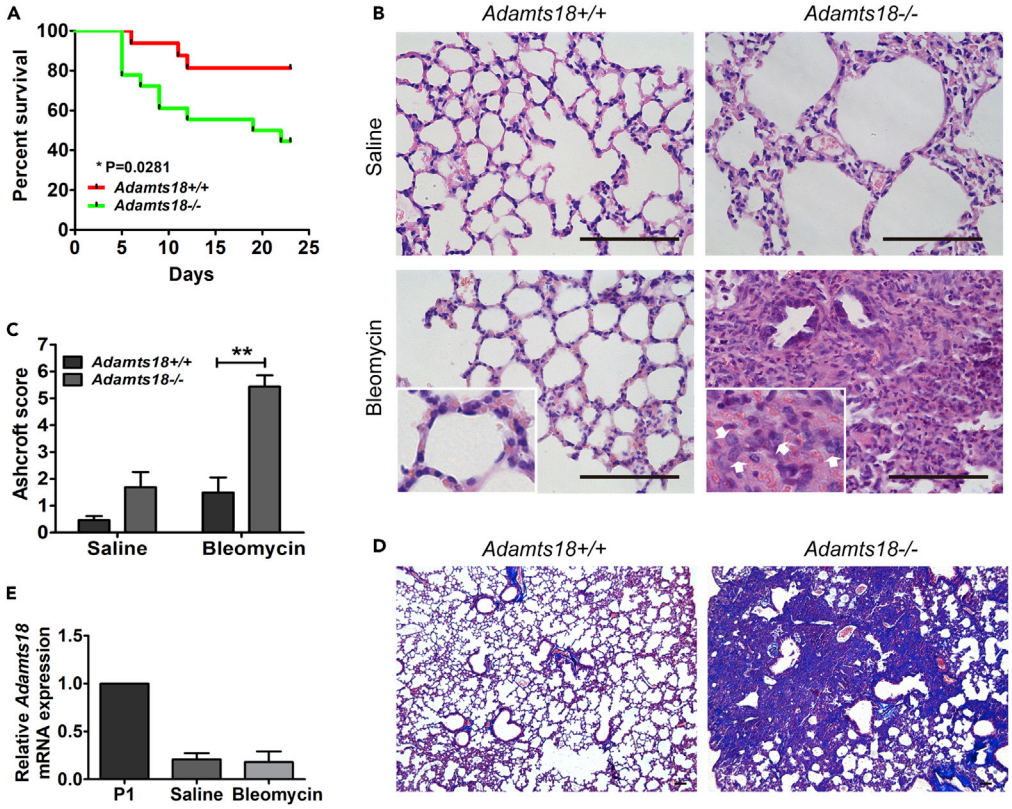

Figure 5. Increased Susceptibility of *Adamts18*$^{-/-}$ Mice to Bleomycin-Induced Lung Fibrosis

(A) Log rank curves of 8-week-old *Adamts18*$^{+/+}$ and *Adamts18*$^{-/-}$ male mice challenged with bleomycin (n = 19/group, *p < 0.05).

(B) Representative images of lung sections of saline-treated (upper panels) or bleomycin-treated (lower panels) mice. Increased inflammation in *Adamts18*$^{-/-}$ lung sections is revealed by H&E staining (lower panel, white arrows). Scale bar, 100 μm.

(C) Ashcroft scoring of lung fibrosis in mice 23 days after treatment with bleomycin or saline. Results are expressed as mean ± SD (n = 4/group, **p < 0.01, Student's t test).

(D) Masson's trichrome staining for aggregated collagen deposition in lung sections of bleomycin-treated *Adamts18*$^{-/-}$ mice. Scale bar, 100 μm.

(E) Relative mRNA levels of *Adamts18* in lungs of saline or bleomycin-treated mice determined by quantitative real-time RT-PCR. P1 mouse lung serves as the negative control. Data are expressed as mean ± SEM (n = 3).

were comparable to those in *Adamts18*$^{+/+}$ lungs (Figure 6D). These observations suggest that the increase in FBN1 protein level in *Adamts18*$^{-/-}$ lungs was not due to an increase in *Fbn1* mRNA transcription.

Interaction between ADAMTS18 and FBN Proteins

To investigate whether ADAMTS18 binds to fibrillins, HEK293T cells transiently transfected with *Adamts18-myc-ddk* were seeded on mouse dermal fibroblast cells (DFCs), which provided FBN1 and FBN2 proteins *in vitro* (Figure 6E). ADAMTS18 was found to co-localize with both exogenous FBN1 and FBN2 proteins. Co-immunoprecipitation (co-IP) was then performed to confirm the interaction between ADAMTS18 and fibrillins. Cell lysates of co-cultures of *Adamts18-myc-ddk* transfected 293T cells and DFCs were incubated overnight with anti-DDK (FLAG tag) agarose beads. A 180-kDa band of ADAMTS18-MYC-DDK was observed by western blotting, and no band in the sample of untransfected cells was seen. FBN1 was pulled down by ADAMTS18 and detected with anti-FBN1-C-terminal antibody, whereas there was no co-IP of FBN2 with ADAMTS18 (Figure 6F). This result suggests that ADAMTS18 binds to FBN1.

Recovery of *Adamts18*$^{-/-}$ Lung Morphogenesis by Inhibiting FBN Expression

To investigate whether decreasing the abundance of FBN1 or FBN2 in mutant lungs could rescue their branching defects, *Fbn1* or *Fbn2* antisense (AS)-phosphorothioated oligodeoxynucleotides (ODNs) were

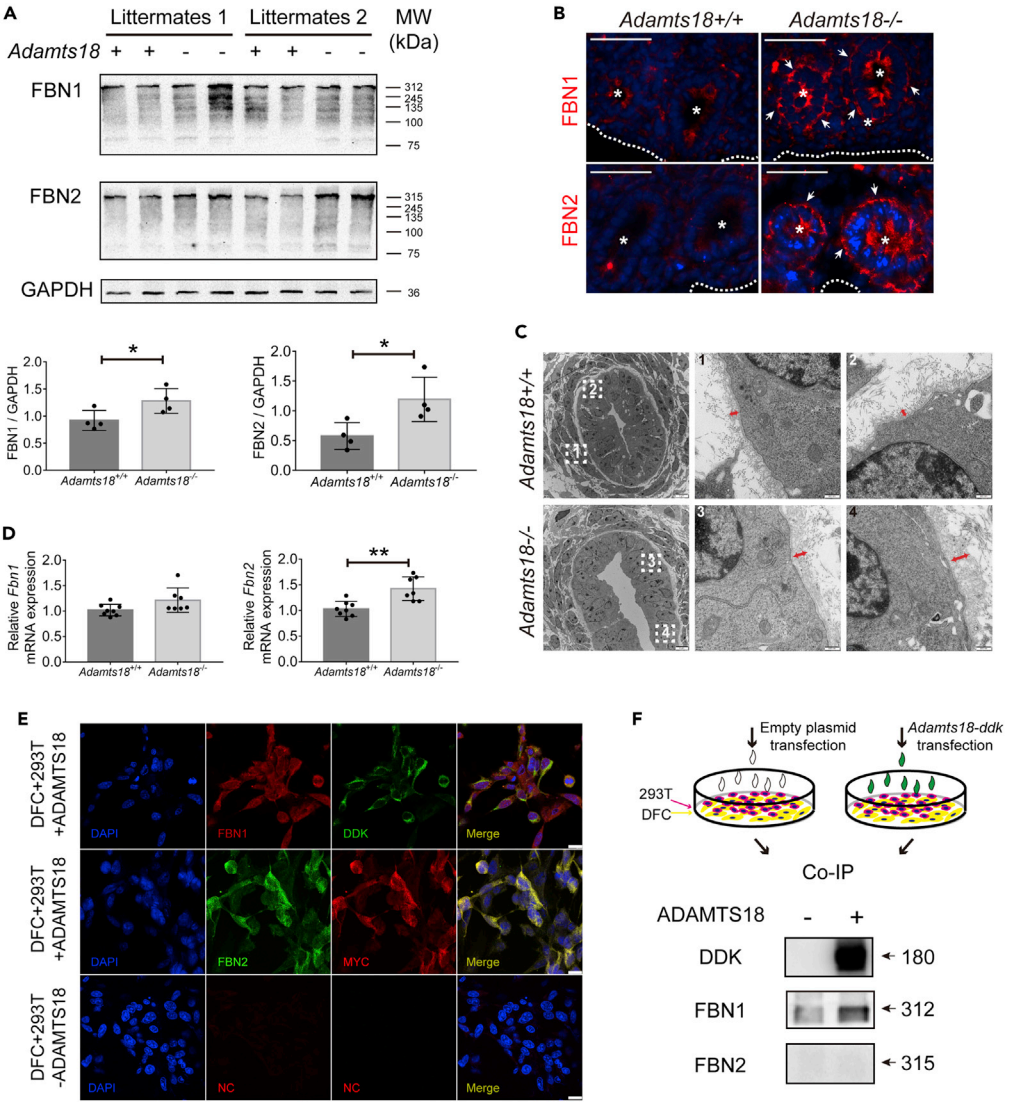

Figure 6. Interactions between ADAMTS18 and Fibrillins

(A) Western blotting results of FBN1 and FBN2 in E14.5 lungs of *Adamts18*$^{+/+}$ and *Adamts18*$^{-/-}$ mice. The relative quantity of FBN1 and FBN2 proteins is normalized to that of GAPDH and expressed as mean ± SD (n = 4).

(B) Representative immunohistochemical images of FBN1 and FBN2 in E14.5 lung sections. * denote distal airways, and white arrows indicate FBN1 or FBN2 distribution around distal airways. White dotted curves mark visceral pleura. Scale bar, 100 μm.

(C) Transmission electron microscopic images of E14.5 lungs. 1, 2 and 3, 4 are selected fields of the basement membrane of *Adamts18*$^{+/+}$ and *Adamts18*$^{-/-}$ lungs. The lengths of red arrows indicate the thickness of the microfibril layer outside the lamina dense.

(D) Relative mRNA levels of *Fbn1* and *Fbn2* determined by real-time RT-PCR. The levels of *Fbn1* and *Fbn2* mRNAs are normalized to those of the housekeeping gene *Gapdh* using the *ΔΔCt* method. Data are expressed as mean ± SEM (n = 7).

(E) Colocalization of ADAMTS18 and fibrillins. *Adamts18-myc-ddk* transiently transfected HEK293T cells were co-cultured with or without mouse dermal fibroblasts (DFCs) and stained with DAPI (blue), anti-FBN1 (red), anti-FBN2 (green), and antibodies against DDK (green) or MYC (red) to label ADAMTS18. Merged yellow sites showed co-localization of ADAMTS18 and FBN1 or FBN2. Scale bar, 100 μm.

(F) Western blotting results of co-IP. *$p < 0.05$, **$p < 0.01$. These experiments were repeated independently at least three times.

See also Figures S3 and S4, Tables S3 and S4.

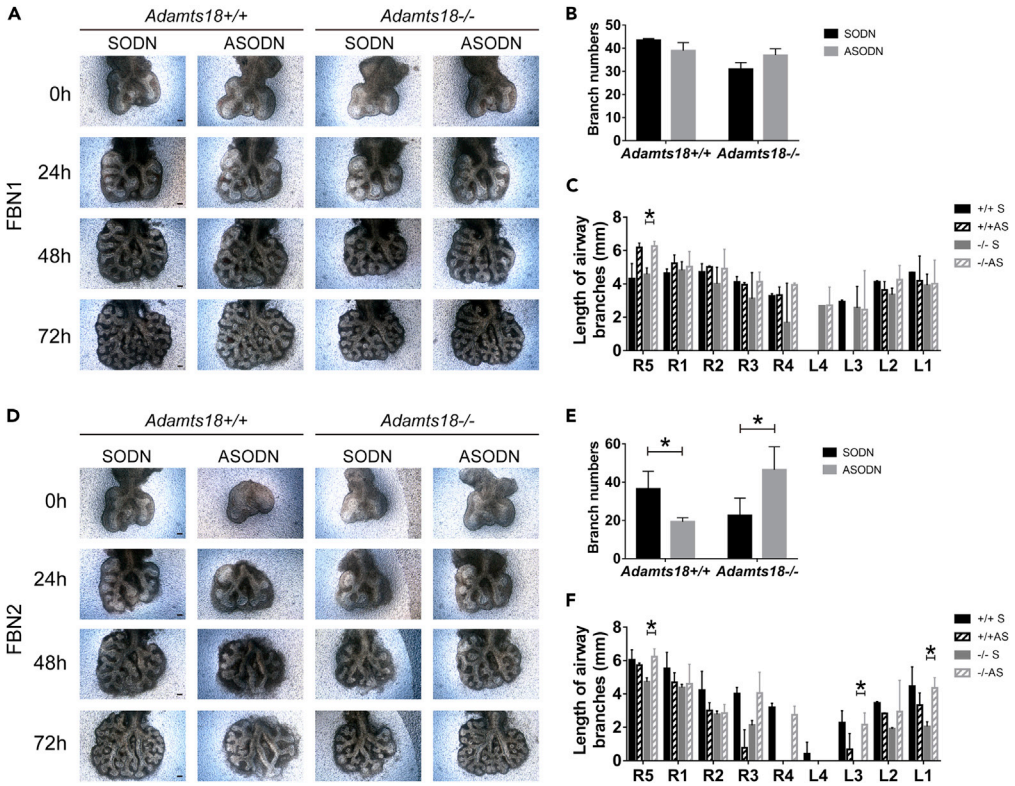

Figure 7. Restoration of *Adamts18*$^{-/-}$ Lung Branching Morphogenesis by *Fbn1* or *Fbn2* Sense (Control) and Antisense Oligonucleotides (ASODN) in Lung Explants

(A and D) E11.5 lungs were cultured *in vitro* and photographed at 0, 24, 48, and 72 h. 0.5 μM *Fbn1* ODN or 1 μM *Fbn2* ODN was added to the cultures every 24 h. Scale bar, 100 μm.

(B and E) Branch number of lungs cultured for 72 h.

(C and F) Lengths of L1-L5 and R1-R5 bronchi of 72 h-cultured explants. SODN, sense oligonucleotides. ASODN, antisense oligonucleotides. Results are expressed as mean ± SD, n = 3 (*p < 0.05). These experiments were repeated independently at least three times.

added to lung explant cultures (Figure 7). For lung explants of *Adamts18*$^{+/+}$ mice, *Fbn1* ASODN treatment had little effect on airway branching; however, *Fbn2* ASODN induced dysmorphogenesis of the lung explants, including reduced number of branches and decreased length of secondary bronchi, as previously reported (Yang et al., 1999). For lung explants of *Adamts18*$^{-/-}$ mice, *Fbn1* ASODN treatment partially restored the length of secondary bronchi resulting in a profound increase in the length of R5 secondary bronchi. Treatment with *Fbn2* ASODN resulted in increased number of branches and lengths of R5, L3, and L1 secondary bronchi.

Altered Cytoskeleton Signaling in *Adamts18*$^{-/-}$ Lungs

In addition to fibrillins, other ECM proteins involved in branching were also examined (Table S3). Some of these ECM proteins, such as Col1a2, Col3a1, Lama1, Lama3, Lamb1, Lamc1, dystroglycan, nidogen1, and Ctgf, showed significant difference in mRNA or protein levels between the two genotypes of mice.

ECM provides mechanical strength to the epithelium and induces new branches in the lungs. The mechanical signal is transduced in part by the focal adhesion kinase (FAK) in lung epithelial cells (Gjorevski and Nelson, 2010). By IHC analyses, total FAK levels in *Adamts18*$^{+/+}$ and *Adamts18*$^{-/-}$ lungs were found to be similar, but the levels of Tyr297-phosphorylated FAK were lower in lung epithelial cells of *Adamts18*$^{-/-}$ mice (Figure 8A). The RhoA GTPase, which regulates cell cytoskeleton arrangement in conjunction with FAK (Provenzano and Keely, 2011), also showed a lower activation level in *Adamts18*$^{-/-}$ lungs (Figure 8B). In proteomic study, 43 proteins involved in supramolecular fiber organization were found to be differentially expressed, most of which were involved in F-actin filament assembly (Table S2). The level

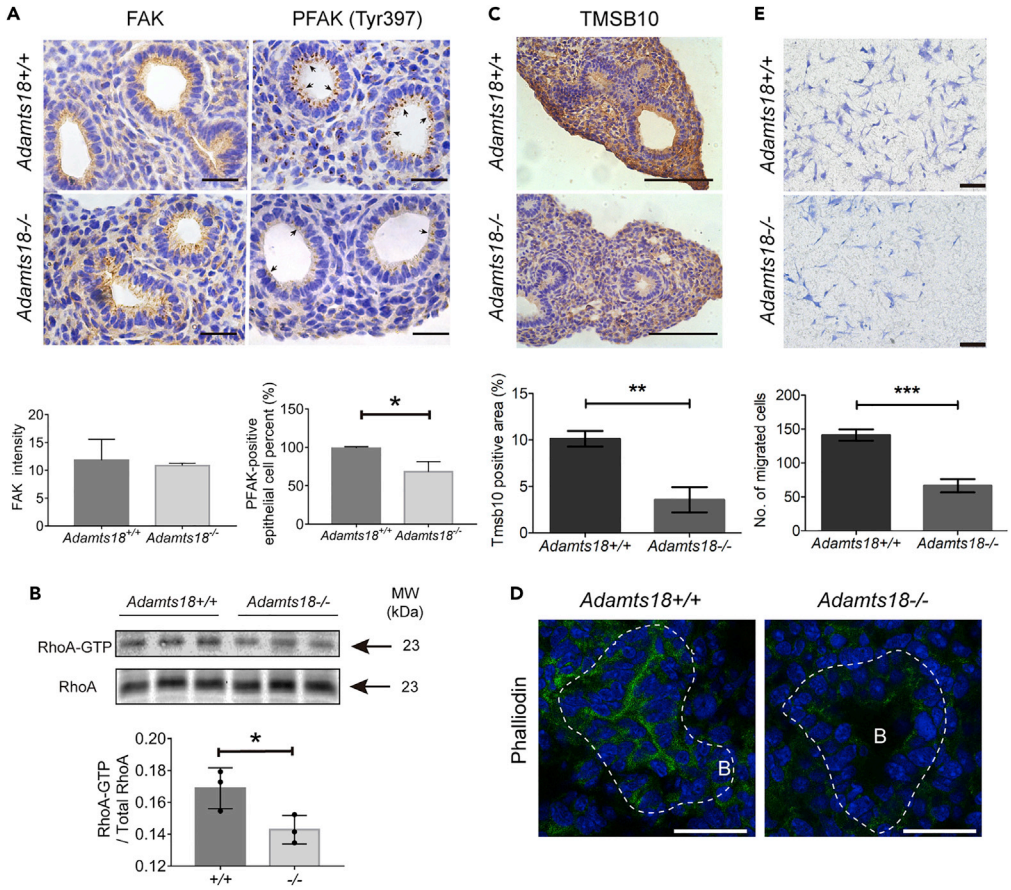

Figure 8. Reduced Amount of phosphorylated FAK (PFAK) and Altered Cytoskeleton in *Adamts18*$^{-/-}$ Lungs

(A) IHC results of Tyr397-PFAK and total FAK of E14.5 lungs. Scale bar, 50 μm. Determination of the intensity of FAK staining and the percentage of Tyr397-PFAK-positive epithelial cell was performed with Image Pro Plus. Scale bar, 100 μm.

(B) GTP-bound RhoA in E15.5 lungs was precipitated with Rhotekin and analyzed by western blotting for RhoA. RhoA-GTP was quantified relative to total RhoA protein.

(C) Representative images of anti-TMSB10 IHC at E14.5. Quantification of TMSB10-positive areas was performed with Image Pro Plus. Scale bar, 100 μm.

(D) Representative images of phalloidin-stained E14.5 lung sections. White dotted lines indicate the boundary of distal epithelium. B, bronchiole. Scale bar, 20 μm.

(E) Transwell analysis of mouse embryonic fibroblasts (MEFs) from *Adamts18*$^{+/+}$ or *Adamts18*$^{-/-}$ mice. Data are expressed as mean ± SEM (n = 3). *p < 0.05, **p < 0.01, ***p < 0.001.

See also Table S2.

of the cytoskeleton protein Tmsb10, which binds and stabilizes G-actin (Fanni et al., 2011), was found to be significantly decreased (0.3-fold) in *Adamts18*$^{-/-}$ lungs. This result was confirmed by IHC (Figure 8C). Phalloidin staining showed less F-actin distribution on the apical surface of the epithelial cells facing the lumen in *Adamts18*$^{-/-}$ lungs (Figure 8D). These data indicate that ADAMTS18 deficiency caused F-actin disorganization, which may result in reduced cell mobility. *In vitro* transwell assays showed a significant decrease in the migration of E14.5 *Adamts18*$^{-/-}$ mouse embryonic fibroblasts (MEFs) compared with *Adamts18*$^{+/+}$ lung MEFs (Figure 8E).

DISCUSSION

ADAMTS18 is a poorly characterized member of the ADAMTS family of metalloproteinases. Previously, Ataca et al. created *Adamts18*$^{-/-}$ C57Bl6/Ola mice in which exons 8–9 of the *Adamts18* gene was deleted and found that these mice have a higher percentage of adjacent bronchioles and larger airspaces with thinner walls (Ataca et al., 2016). Recently, Rudge et al. generated another strain of *Adamts18*$^{-/-}$ mice (VG12442) by deleting a 3,616-bp fragment encompassing the region between the ATG codon in exon 1

and the end of exon 3 (Rutledge et al., 2019). They found that these *Adamts18*$^{-/-}$ mice have shorter primary branches but maintain the ability to form secondary lateral branches in E12.5 lungs. These findings indicate that ADAMTS18 is crucial for early lung development. However, the mechanisms by which ADAMTS18 affects lung morphogenesis and the effect of ADAMTS18 deficiency on lung function remain largely unknown. In this study, we performed experiments using another *Adamts18*$^{-/-}$ mouse strain with the C57BL6/126SV background. In this mouse strain, exons 5–6 of the *Adamts18* gene are deleted (Lu et al., 2017). These *Adamts18*$^{-/-}$ mice exhibit reduced numbers and lengths of bronchi, tipped lung apexes, and dilated alveoli. These developmental defects worsen LPS-induced acute lung injury and bleomycin-induced lung fibrosis in adult *Adamts18*$^{-/-}$ mice. By examining the bronchial ECM of these mice, we revealed a novel function of ADAMTS18 in modulating fibrillin microfibril formation.

Mouse microfibril is mainly composed of FBN1 and FBN2. Our results showed that *Adamts18*$^{-/-}$ lungs had more microfibrils in the basement membrane surrounding the distal airway at E14.5 (Figures 6A–6C). The accumulation of microfibrils in the bronchial wall of *Adamts18*$^{-/-}$ mice was mainly due to increased FBN2 expression (Figures 6A and 6B). Inhibition of FBN1 or FBN2 expression by ASODNs revealed that FBN2 plays a more important role than FBN1 in early bronchial development (Figure 7). Similar to our findings, Hubmacher et al. found that *Adamtsl2* deletion results in bronchial fibrillin microfibril accumulation due to increased FBN2 deposition on the bronchial wall (Hubmacher et al., 2015). *Adamtsl2* deletion increases bronchial FBN2 expression only at protein level, and *Adamtsl2* is shown to bind directly to FBN2. However, our data showed that FBN2 levels were increased at both protein and mRNA levels in the lungs of *Adamts18*$^{-/-}$ mice (Figures 6A, 6B, and 6D), suggesting that the increased FBN2 expression is due to enhanced *Fbn2* mRNA transcription. It is possible that ADAMTS18 directly processes certain ECMs of microfibril networks, such as FBN1, thus altering tissue stiffness and mechano-signaling and resulting in secondary transcription of other ECM protein genes. In addition to altered *Fbn2* mRNA levels, we have previously observed increased *laminin* transcription in *Adamts18*$^{-/-}$ adipose tissue and embryonic brains affecting early adipocyte differentiation and neurite formation (Zhu et al., 2018, 2019). This possibility was further indicated by the finding that ADAMTS18 regulates mammary stem cell niche by cleaving fibronectin. This action may lead to changes in the abundance of collagen I, collagen IV, laminin, and collagen XVIII (Ataca et al., 2020).

In this study, we found that ADAMTS18 co-localizes with both FBN1 and FBN2 in the ECM of cultured fibroblasts (Figure 6E). Co-IP results showed that FBN1, but not FBN2, was pulled down by ADAMTS18 (Figure 6F). These data suggest that ADAMTS18 binds to FBN1. Similar to our findings, previous studies showed that some ADAMTS and ADAMTSL proteases can bind to FBN1 or FBN2 or both. Among them, ADAMTS10 has two FBN1 binding sites and binds to both the N (exons 8–11) and C termini of FBN1 (Hubmacher and Apte, 2011; Kutz et al., 2011). ADAMTS6 has been shown to bind to an N-terminal region of FBN1 (exons 8–11) (Cain et al., 2016). ADAMTS17 binds to both FBN1 and FBN2 (Hubmacher et al., 2017). ADAMTSL2, ADAMTSL4, and ADAMTSL6 are known to bind FBN1 (Gabriel et al., 2012; Le Goff et al., 2011; Tsutsui et al., 2010). ADAMTSL5 has been shown to bind both FBN1 and FBN2 (Bader et al., 2012). We speculate that ADAMTS18 forms a complex with FBN1 and regulates the activity of FBN2 in the fibrillin microfibril scaffold. Because of technical difficulties (Mead and Apte, 2018), we have yet to purify full-length ADAMTS18 proteins for further affinity analysis.

Fibrillin microfibrils represent pivotal ECM signaling platforms integrating the functions of transforming growth factor β, bone morphogenetic protein (BMP), and mechano-signaling (Ramirez and Sakai, 2010). ECM mechanical properties are affected by elastic fibers, fibrillar collagens, glycosaminoglycans, and related proteoglycans. Fibrillar collagens provide tissue stiffness and strength, whereas microfibril-containing elastic fibers are associated with extensibility and resilience (Humphrey et al., 2014). Thus, increased microfibril composition in ECM results in a compliant matrix. Surrounding cells sense the mechanics of ECM through integrins, focal adhesions proteins, and actomyosin cytoskeleton. It has been demonstrated that the phosphorylation level of FAK increases in response to changes in the stiffness of ECM (Du et al., 2016), and FAK signaling is suppressed in compliant ECM (Humphrey et al., 2014). Therefore, ADAMTS18 deficiency increases the levels of fibrillin and tissue compliance, resulting in down regulation of FAK signaling.

Epithelial-mesenchymal transition (EMT) also plays key roles in lung development. BMP, WNT, and FGF signaling induce EMT during branching morphogenesis (Nieto et al., 2016). We found that mRNA levels

of *Bmp4*, *Wnt2*, and *Fgf10* in lung tissues of *Adamts18*$^{+/+}$ and *Adamts18*$^{-/-}$ mice were similar (Figure S2) and that those of *Fgfr2* were significantly increased in *Adamts18*$^{-/-}$ lungs compared with *Adamts18*$^{+/+}$ lungs (Figure S2). These pathways can activate one or more EMT-driving transcription factors such as SNAIL1 and SNAIL2 (Nieto et al., 2016). However, *Snail1* and *Snail2* mRNA levels showed no difference in *Adamts18*$^{+/+}$ and *Adamts18*$^{-/-}$ lung tissues (Figure S5A). The hallmark of EMT is loss of epithelial cell-cell adhesion molecule E-cadherin and/or concomitant expression of mesenchymal markers such as N-cadherin, vimentin, and alpha-smooth muscle actin (Nieto et al., 2016). The expression levels of *E-cadherin*, *N-cadherin*, and *Vimentin* also showed no difference in lung tissues of *Adamts18*$^{+/+}$ and *Adamts18*$^{-/-}$ mice (Figure S5B). Reorganization of the actin cytoskeleton and activation of the RhoA GTPase equip epithelial cells with the mesenchymal traits of migration. Although major EMT biomarkers detected were not changed in *Adamts18*$^{-/-}$ lungs, *Adamts18*$^{-/-}$ distal epithelial cells showed fewer F-actin bundles and reduced activation of RhoA GTPase during branching morphogenesis, suggesting diminished migratory property of terminal epithelial cells and EMT involvement.

The lungs of *Adamts18*$^{-/-}$ mice exhibited several structural defects, including linear atelectasis and dilated alveoli with decreased number of RACs (Figure 3D). As *Adamts18* mRNA is not expressed at the alveolization stage, these lung defects are likely the secondary effect of bronchodysplasia. We observed a thicker elastin layer on alveolar walls of *Adamts18*$^{-/-}$ lungs than those of *Adamts18*$^{+/+}$ lungs (Figures 3E and S1). Normally, elastin is distributed in alveolar tips and guides the formation of alveoli (Zhou et al., 2018). It is likely that excessive fibrillin accumulation in mice with ADAMTS18 deficiency promotes elastic fiber synthesis, leading to increased elastin production and ectopic elastin deposition on alveolar walls.

In the study of LPS-induced acute lung injury and bleomycin-induced lung fibrosis, adult *Adamts18*$^{-/-}$ mice demonstrated a high susceptibility to lung inflammation and fibrosis (Figures 4 and 5). LPS treatment may induce production and release of proinflammatory cytokines IL-1, tumor necrosis factor-α, IL-6, and chemokines (IL-8 and macrophage inflammatory protein-2), leading to recruitment of neutrophils and acute lung injury (Moreland et al., 2002). Although release of NETs was not observed in both *Adamts18*$^{+/+}$ and *Adamts18*$^{-/-}$ mice 24 h after LPS injection, increased capillary permeability, interstitial edema, and more serious tissue damages were clearly observed in *Adamts18*$^{-/-}$ lungs. These symptoms may be due to elevated levels of the proinflammatory cytokine IL-6 and infiltration of CD11b^{+} neutrophils.

Taken together, results of this study indicate that ADAMTS18 is secreted by bronchial epithelial cells and binds to FBN1. *In vivo*, ADAMTS18 deficiency causes increased levels of FBN1 and FBN2 and accumulation of microfibrils in bronchi. Accumulation of microfibrils causes a weakened FAK signaling and abnormal F-actin organizations. *In vitro*, ADAMTS18 deficiency causes a reduction in the migration of embryonic fibroblasts.

Limitations of the Study

In the present study, we demonstrated that ADAMTS18 regulates early lung development in a microfibril-dependent manner by binding to fibrillin1 protein. However, the binding site of ADAMTS18 on fibrillin1 and how it affects fibrillin abundance remain to be investigated.

Resource Availability

Lead Contact

Further information and requests for resources and reagents will be fulfilled by the Lead Contact, Wei Zhang (wzhang@sat.ecnu.edu.cn).

Materials Availability

This study did not generate new unique reagents.

Data and Code Availability

The raw data of this article are available from the leading contact upon request.

METHODS

All methods can be found in the accompanying Transparent Methods supplemental file.

SUPPLEMENTAL INFORMATION

Supplemental Information can be found online at https://doi.org/10.1016/j.isci.2020.101472.

ACKNOWLEDGMENTS

This work was supported by grants from the National Natural Science Foundation of China (NSFC) (No. 81770139, 81570389 and 81170481 to W.Z.) and the Shanghai Municipal Natural Science Foundation (16ZR1423700 to S.D.). We thank Dr. Chao-Hung Lee for editing the manuscript and providing valuable advices.

AUTHOR CONTRIBUTIONS

T.L., S.D., and W.Z. conceived the study and designed the experiments. T.L., X.L., and C.W. performed experiments and analyzed data. S.Y., Q.Z., and T.Z. genotyped mice and maintained mouse colonies. R.Z., Y.-H.P., T.M.W., Z.C., and B.-S.D. provided valuable advices. T.L. and W.Z. wrote the manuscript.

DECLARATION OF INTERESTS

The authors declare that they have no conflict of interest.

Received: November 4, 2019
Revised: July 2, 2020
Accepted: August 17, 2020
Published: September 25, 2020

REFERENCES

Aldahmesh, M.A., Khan, A.O., Mohamed, J.Y., Alkuraya, H., Ahmed, H., Bobis, S., Al-Mesfer, S., and Alkuraya, F.S. (2011). Identification of ADAMTS18 as a gene mutated in Knobloch syndrome. J. Med. Genet. *48*, 597–601.

Aldahmesh, M.A., Alshammari, M.J., Khan, A.O., Mohamed, J.Y., Alhabib, F.A., and Alkuraya, F.S. (2013). The syndrome of microcornea, myopic chorioretinal atrophy, and telecanthus (MMCAT) is caused by mutations in ADAMTS18. Hum. Mutat. *34*, 1195–1199.

Ataca, D., Aouad, P., Constantin, C., Laszlo, C., Beleut, M., Shamseddin, M., Rajaram, R.D., Jeitziner, R., Mead, T.J., Caikovski, M., et al. (2020). The secreted protease Adamts18 links hormone action to activation of the mammary stem cell niche. Nat. Commun. *11*, 1571.

Ataca, D., Caikovski, M., Piersigilli, A., Moulin, A., Benarafa, C., Earp, S.E., Guri, Y., Kostic, C., Arsenijevic, Y., Soininen, R., et al. (2016). Adamts18 deletion results in distinct developmental defects and provides a model for congenital disorders of lens, lung, and female reproductive tract development. Biol. Open *5*, 1585–1594.

Bader, H.L., Wang, L.W., Ho, J.C., Tran, T., Holden, P., Fitzgerald, J., Atit, R.P., Reinhardt, D.P., and Apte, S.S. (2012). A disintegrin-like and metalloprotease domain containing thrombospondin type 1 motif-like 5 (ADAMTSL5) is a novel fibrillin-1-, fibrillin-2-, and heparin-binding member of the ADAMTS superfamily containing a netrin-like module. Matrix Biol. *31*, 398–411.

Cain, S.A., Mularczyk, E.J., Singh, M., Massam-Wu, T., and Kielty, C.M. (2016). ADAMTS-10 and -6 differentially regulate cell-cell junctions and focal adhesions. Sci. Rep. *6*, 35956.

Di Valentin, E., Crahay, C., Garbacki, N., Hennuy, B., Gueders, M., Noel, A., Foidart, J.M., Grooten, J., Colige, A., Piette, J., et al. (2009). New asthma biomarkers: lessons from murine models of acute and chronic asthma. Am. J. Physiol. Lung Cell. Mol. Physiol. *296*, L185–L197.

Du, J., Zu, Y., Li, J., Du, S., Xu, Y., Zhang, L., Jiang, L., Wang, Z., Chien, S., and Yang, C. (2016). Extracellular matrix stiffness dictates Wnt expression through integrin pathway. Sci. Rep. *6*, 20395.

Fanni, D., Gerosa, C., Nemolato, S., Locci, A., Marinelli, V., Cabras, T., Messana, I., Fanos, V., Castagnola, M., and Faa, G. (2011). Thymosin beta 10 expression in developing human salivary glands. Early Hum. Dev. *87*, 779–783.

Gabriel, L.A., Wang, L.W., Bader, H., Ho, J.C., Majors, A.K., Hollyfield, J.G., Traboulsi, E.I., and Apte, S.S. (2012). ADAMTSL4, a secreted glycoprotein widely distributed in the eye, binds fibrillin-1 microfibrils and accelerates microfibril biogenesis. Invest. Ophthalmol. Vis. Sci. *53*, 461–469.

Gjorevski, N., and Nelson, C.M. (2010). Endogenous patterns of mechanical stress are required for branching morphogenesis. Integr. Biol. *2*, 424–434.

He, H., Huang, M., Sun, S., Wu, Y., and Lin, X. (2017). Epithelial heparan sulfate regulates Sonic Hedgehog signaling in lung development. PLoS Genet. *13*, e1006992.

Hubmacher, D., and Apte, S.S. (2011). Genetic and functional linkage between ADAMTS superfamily proteins and fibrillin-1: a novel mechanism influencing microfibril assembly and function. Cell. Mol. Life Sci. *68*, 3137–3148.

Hubmacher, D., Schneider, M., Berardinelli, S.J., Takeuchi, H., Willard, B., Reinhardt, D.P., Haltiwanger, R.S., and Apte, S.S. (2017). Unusual life cycle and impact on microfibril assembly of ADAMTS17, a secreted metalloprotease mutated in genetic eye disease. Sci. Rep. *7*, 41871.

Hubmacher, D., Wang, L.W., Mecham, R.P., Reinhardt, D.P., and Apte, S.S. (2015). *Adamtsl2* deletion results in bronchial fibrillin microfibril accumulation and bronchial epithelial dysplasia – a novel mouse model providing insights into geleophysic dysplasia. Disease Models & Mechanisms *8*, 487–499.

Humphrey, J.D., Dufresne, E.R., and Schwartz, M.A. (2014). Mechanotransduction and extracellular matrix homeostasis. Nat. Rev. Mol. Cell Biol. *15*, 802–812.

Jin, H., Wang, X., Ying, J., Wong, A.H., Li, H., Lee, K.Y., Srivastava, G., Chan, A.T., Yeo, W., Ma, B.B., et al. (2007). Epigenetic identification of ADAMTS18 as a novel 16q23.1 tumor suppressor frequently silenced in esophageal, nasopharyngeal and multiple other carcinomas. Oncogene *26*, 7490–7498.

Jungers, K.A., Le Goff, C., Somerville, R.P., and Apte, S.S. (2005). Adamts9 is widely expressed during mouse embryo development. Gene Expr. Patterns *5*, 609–617.

Kugler, M.C., Joyner, A.L., Loomis, C.A., and Munger, J.S. (2015). Sonic hedgehog signaling in the lung. From development to disease. Am. J. Respir. Cell Mol. Biol. *52*, 1–13.

Kurz, T., Hoffjan, S., Hayes, M.G., Schneider, D., Nicolae, R., Heinzmann, A., Jerkic, S.P., Parry, R., Cox, N.J., Deichmann, K.A., et al. (2006). Fine mapping and positional candidate studies on chromosome 5p13 identify multiple asthma

susceptibility loci. J. Allergy Clin. Immunol. *118*, 396–402.

Kutz, W.E., Wang, L.W., Bader, H.L., Majors, A.K., Iwata, K., Traboulsi, E.I., Sakai, L.Y., Keene, D.R., and Apte, S.S. (2011). ADAMTS10 protein interacts with fibrillin-1 and promotes its deposition in extracellular matrix of cultured fibroblasts. J. Biol. Chem. *286*, 17156–17167.

Le Goff, C., Mahaut, C., Wang, L.W., Allali, S., Abhyankar, A., Jensen, S., Zylberberg, L., Collod-Beroud, G., Bonnet, D., Alanay, Y., et al. (2011). Mutations in the TGFβ binding-protein-like domain 5 of FBN1 are responsible for acromicric and geleophysic dysplasias. Am. J. Hum. Genet. *89*, 7–14.

Lopez, L.M., Bastin, M.E., Maniega, S.M., Penke, L., Davies, G., Christoforou, A., Valdes Hernandez, M.C., Royle, N.A., Tenesa, A., Starr, J.M., et al. (2012). A genome-wide search for genetic influences and biological pathways related to the brain's white matter integrity. Neurobiol. Aging *33*, 1847.e1–1847.e14.

Lu, T., Dang, S., Zhu, R., Wang, Y., Nie, Z., Hong, T., and Zhang, W. (2017). Adamts18 deficiency promotes colon carcinogenesis by enhancing beta-catenin and p38MAPK/ERK1/2 signaling in the mouse model of AOM/DSS-induced colitis-associated colorectal cancer. Oncotarget *8*, 18979–18990.

Mead, T.J., and Apte, S.S. (2018). ADAMTS proteins in human disorders. Matrix Biol. *71-72*, 225–239.

Moreland, J.G., Fuhrman, R.M., Pruessner, J.A., and Schwartz, D.A. (2002). CD11b and intercellular adhesion molecule-1 are involved in pulmonary neutrophil recruitment in lipopolysaccharide-induced airway disease. Am. J. Respir. Cell Mol. Biol. *27*, 474–480.

Nieto, M.A., Huang, R.Y., Jackson, R.A., and Thiery, J.P. (2016). EMT: 2016. Cell *166*, 21–45.

Paulissen, G., Rocks, N., Quesada-Calvo, F., Gosset, P., Foidart, J.M., Noel, A., Louis, R., and Cataldo, D.D. (2006). Expression of ADAMs and their inhibitors in sputum from patients with asthma. Mol. Med. *12*, 171–179.

Peluso, I., Conte, I., Testa, F., Dharmalingam, G., Pizzo, M., Collin, R.W., Meola, N., Barbato, S., Mutarelli, M., Ziviello, C., et al. (2013). The ADAMTS18 gene is responsible for autosomal recessive early onset severe retinal dystrophy. Orphanet J. Rare Dis. *8*, 16.

Provenzano, P.P., and Keely, P.J. (2011). Mechanical signaling through the cytoskeleton regulates cell proliferation by coordinated focal adhesion and Rho GTPase signaling. J. Cell Sci. *124*, 1195–1205.

Ramirez, F., and Sakai, L.Y. (2010). Biogenesis and function of fibrillin assemblies. Cell Tissue Res. *339*, 71–82.

Rutledge, E.A., Parvez, R.K., Short, K.M., Smyth, I.M., and McMahon, A.P. (2019). Morphogenesis of the kidney and lung requires branch-tip directed activity of the Adamts18 metalloprotease. Dev. Biol. *454*, 156–169.

Somerville, R.P., Jungers, K.A., and Apte, S.S. (2004). Discovery and characterization of a novel, widely expressed metalloprotease, ADAMTS10, and its proteolytic activation. J. Biol. Chem. *279*, 51208–51217.

Stocks, J., Hislop, A., and Sonnappa, S. (2013). Early lung development: lifelong effect on respiratory health and disease. Lancet Respir. Med. *1*, 728–742.

Thai, S.N., and Iruela-Arispe, M.L. (2002). Expression of ADAMTS1 during murine development. Mech. Dev. *115*, 181–185.

Tsutsui, K., Manabe, R., Yamada, T., Nakano, I., Oguri, Y., Keene, D.R., Sengle, G., Sakai, L.Y., and Sekiguchi, K. (2010). ADAMTSL-6 is a novel extracellular matrix protein that binds to fibrillin-1 and promotes fibrillin-1 fibril formation. J. Biol. Chem. *285*, 4870–4882.

Xiong, D.H., Liu, X.G., Guo, Y.F., Tan, L.J., Wang, L., Sha, B.Y., Tang, Z.H., Pan, F., Yang, T.L., Chen, X.D., et al. (2009). Genome-wide association and follow-up replication studies identified ADAMTS18 and TGFBR3 as bone mass candidate genes in different ethnic groups. Am. J. Hum. Genet. *84*, 388–398.

Yang, Q., Ota, K., Tian, Y., Kumar, A., Wada, J., Kashihara, N., Wallner, E., and Kanwar, Y.S. (1999). Cloning of rat fibrillin-2 cDNA and its role in branching morphogenesis of embryonic lung. Dev. Biol. *212*, 229–242.

Zhou, Y., Horowitz, J.C., Naba, A., Ambalavanan, N., Atabai, K., Balestrini, J., Bitterman, P.B., Corley, R.A., Ding, B.S., Engler, A.J., et al. (2018). Extracellular matrix in lung development, homeostasis and disease. Matrix Biol. *73*, 77–104.

Zhu, R., Cheng, M., Lu, T., Yang, N., Ye, S., Pan, Y.H., Hong, T., Dang, S., and Zhang, W. (2018). A disintegrin and metalloproteinase with thrombospondin motifs 18 deficiency leads to visceral adiposity and associated metabolic syndrome in mice. Am. J. Pathol. *188*, 461–473.

Zhu, R., Pan, Y.H., Sun, L., Zhang, T., Wang, C., Ye, S., Yang, N., Lu, T., Wisniewski, T., Dang, S., et al. (2019). ADAMTS18 deficiency affects neuronal morphogenesis and reduces the levels of depression-like behaviors in mice. Neuroscience *399*, 53–64.

iScience, Volume *23*

Supplemental Information

ADAMTS18 Deficiency Leads to Pulmonary Hypoplasia and Bronchial Microfibril Accumulation

Tiantian Lu, Xiaotian Lin, Yi-Hsuan Pan, Ning Yang, Shuai Ye, Qi Zhang, Caiyun Wang, Rui Zhu, Tianhao Zhang, Thomas M. Wisniewski, Zhongwei Cao, Bi-Sen Ding, Suying Dang, and Wei Zhang

Supplemental Figures

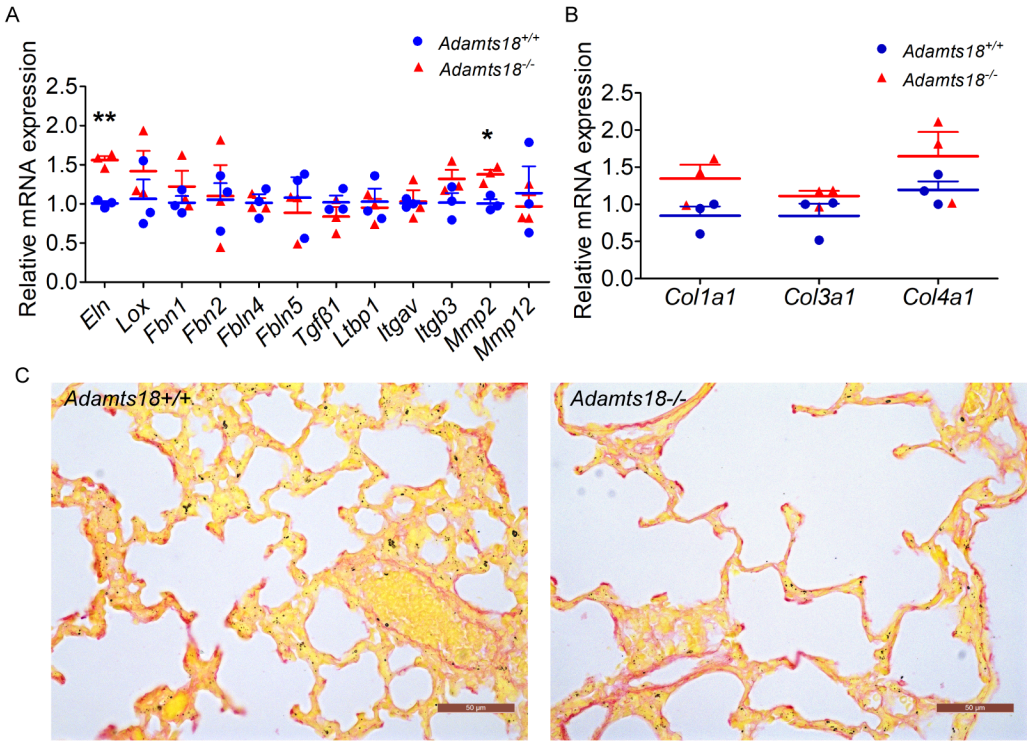

Figure S1. Effect of *Adamts*18 on elastin and collagen in the lungs of two-week-old mice, related to Figure 3 and Table S5. **A)** qRT-PCR results of key proteins involved in elastic fiber synthesis, assembly, and degradation, including *Tropoelastin (Eln)*, *Lox*, *Fibrillin 1 (Fbn1)*, *Fibrllin 2 (Fbn2)*, *Fibulin 4 (Fbln4)*, *Fibulin 5 (Fbln5)*, *Tgfβ1*, *Ltbp1*, *Integrin α5 (Itgα5)*, *Integrin β3 (Itgα3)*, *Mmp2*, and *Mmp12*. **B)** *q*RT-PCR results of *Col1a1*, *Col3a1,* and *Col4a1*. **C)** Lung collagen revealed by Sirius red staining. Scale bar, 50 µm. The relative quantity of target mRNA was normalized to that of the housekeeping gene *Gapdh* using the *ΔΔCt* method. Data are expressed as mean ± s.d. Statistical significance: **P* < 0.05; ***P* < 0.01

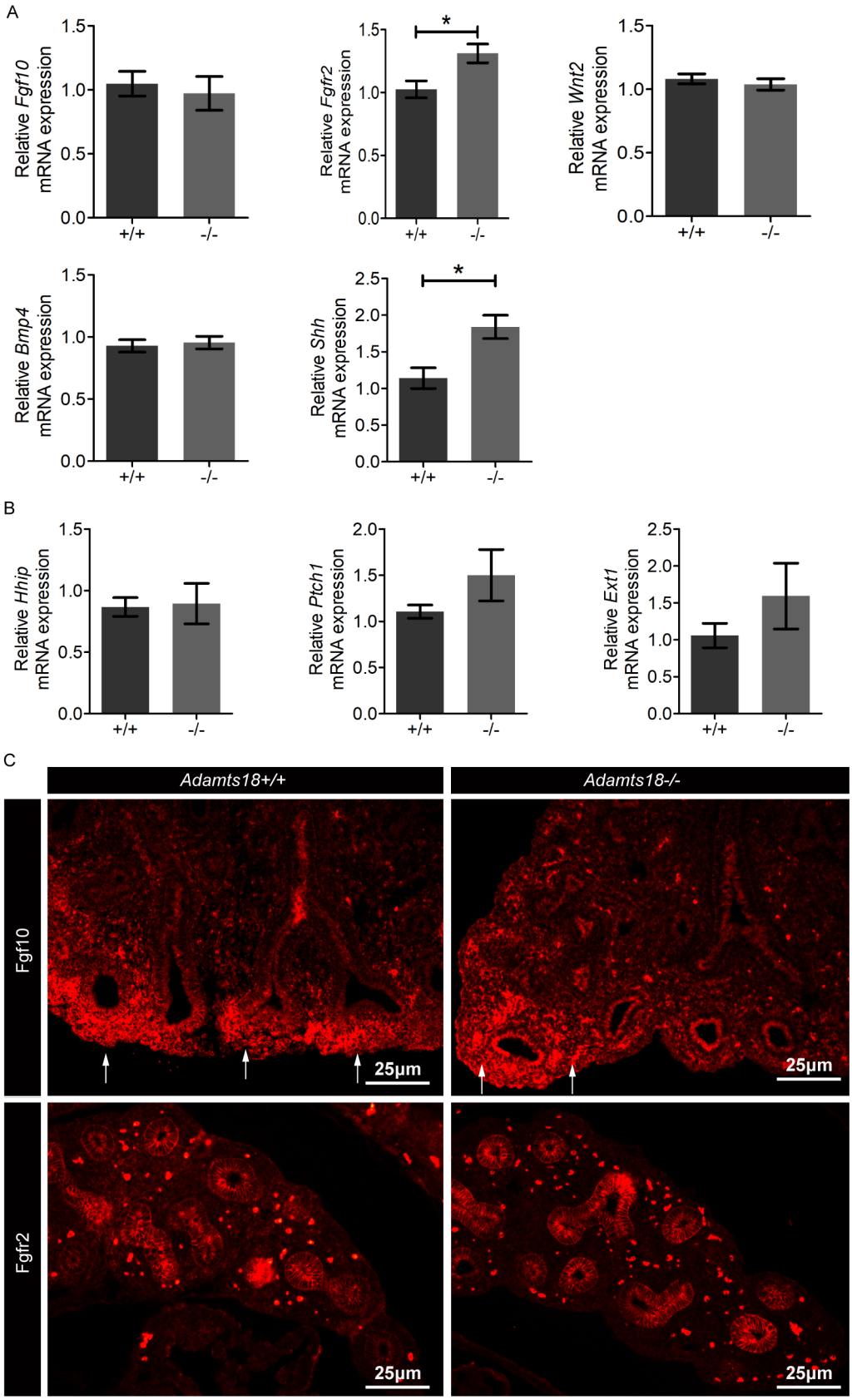

Figure S2. FGF10, Wnt2, Bmp4 and Shh signaling activity in the lungs of *Adamts18*$^{+/+}$ and *Adamts18*$^{-/-}$ mice, related to Figure 2, Table S4 and S5. A-B) Relative mRNA levels of *Fgf10*, *Fgfr2*, *Wnt2*, *Bmp4*, *Shh*, *Hhip*, *Ptch1*, and *Ext1*

determined by *q*RT-PCR. The relative quantity of target mRNA was normalized to that of the housekeeping gene *Gapdh* using the *ΔΔCt* method. Data are expressed as mean ± SEM. **C)** Representative immunostaining images of Fgf10 and Fgfr2 in E14.5 lungs from *Adamts18*$^{+/+}$ and *Adamts18*$^{-/-}$ mice. Scale bar, 25 µm.

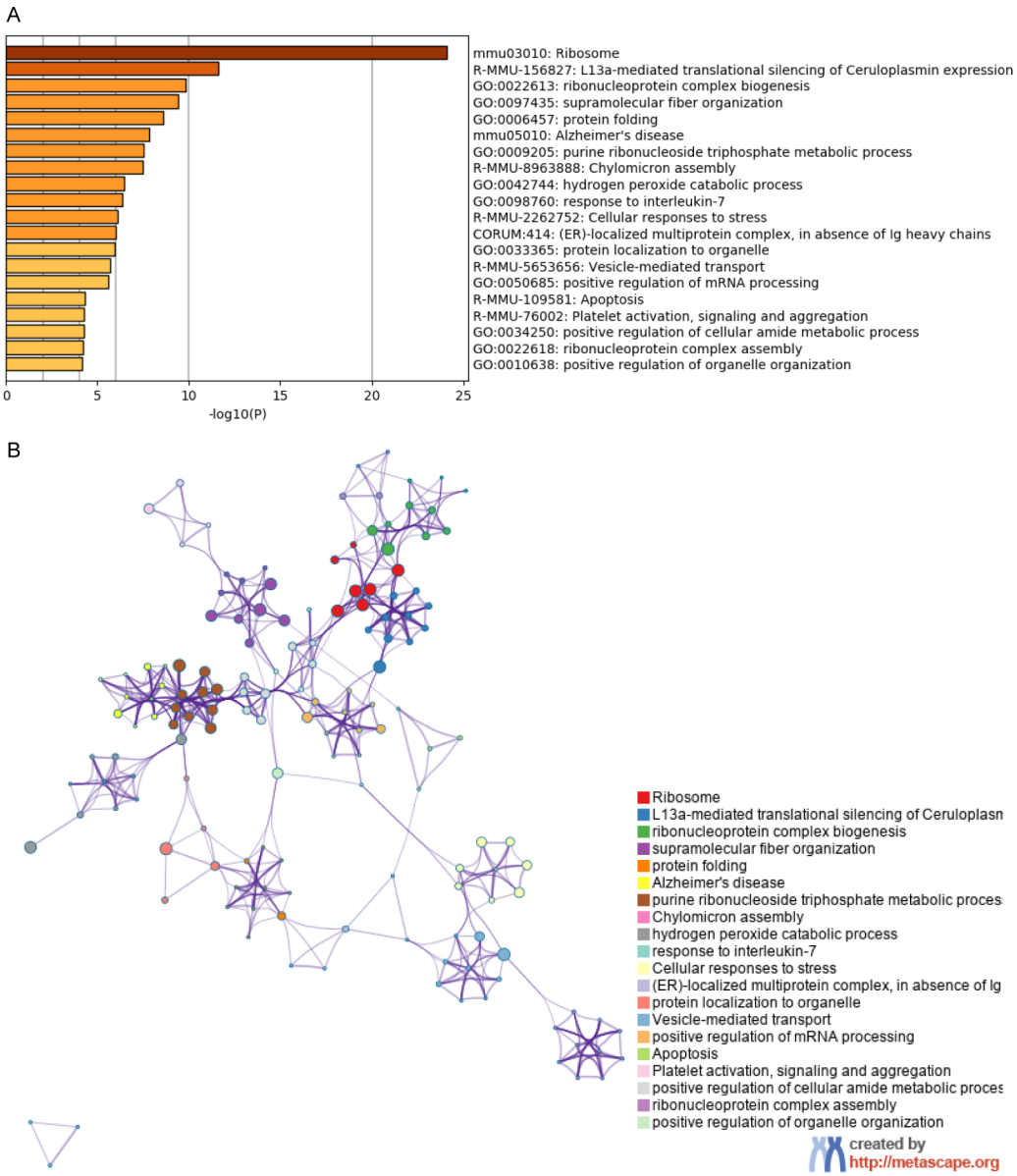

Figure S3. Related to Figure 6. A) Gene ontology (GO) term and pathway analysis. **B)** Protein-protein interactome network analysis of differentially expressed proteins by Metascape.

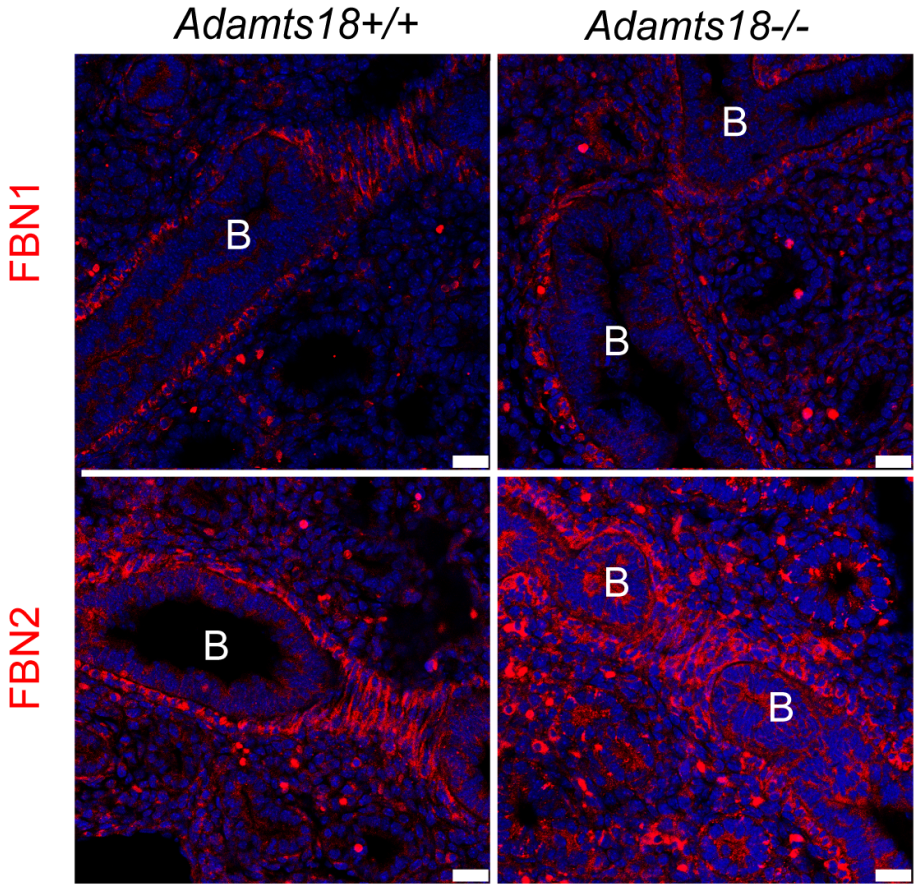

Figure S4. Immunohistochemical localization of fibrillin1 (FBN1) and FBN2 around E14.5 large airways, related to Figure 6 and Table S4. B: bronchi. Scale bar = 200 μm.

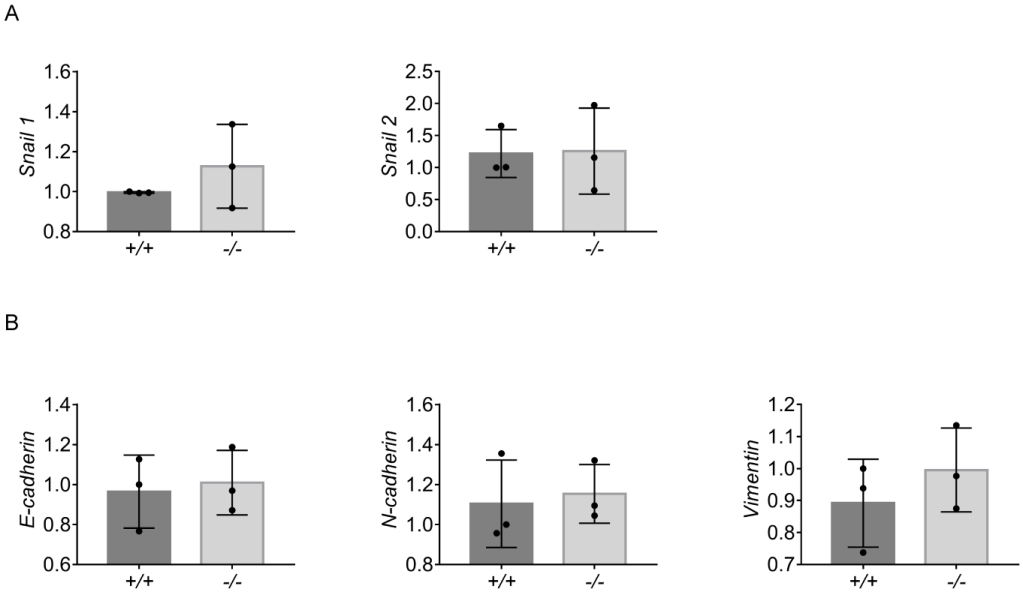

Figure S5. Epithelial–mesenchymal transition (EMT) signaling in the lungs of

***Adamts18*$^{+/+}$ and *Adamts18*$^{-/-}$ mice, related to Figure S3 and Table S5. A-B)**.
Relative mRNA levels of *Snail 1, Snail 2* **(A)**, *E-cadherin (Cdh1)*, *N-cadherin (Cdh2)*, and *Vimentin (Vim)* **(B)** Determination of mRNA levels by *q*RT-PCR. The relative quantity of target mRNA was normalized to that of the housekeeping gene *Gapdh* using the *ΔΔCt* method. Data are expressed as mean ± SEM.

Supplemental Tables

Table S1. Lung functions of 12-week-old mice, related to Figure 3.

	Male			Female		
	Adamts18$^{+/+}$ (n = 6)	*Adamts18*$^{-/-}$ (n = 6)	P value	*Adamts18*$^{+/+}$ (n = 6)	*Adamts18*$^{-/-}$ (n = 6)	P value
Ti (s)	0.23 ± 0.03	0.23 ± 0.08	0.95	0.33 ± 0.09	0.31 ± 0.11	0.94
Te (s)	0.12 ± 0.01	0.12 ± 0.02	0.73	0.12 ± 0.01	0.15 ± 0.04	0.59
f/min	172.16 ± 22.60	184.98 ± 57.09	0.62	136.67 ± 22.87	143.62 ± 53.72	0.78
Phigh (cmH_2O)	25.89 ± 0.34	25.81 ± 6.15	0.75	26.91 ± 0.63	27.26 ± 0.53	0.33
Pmean (cmH_2O)	6.20 ± 0.08	6.15±0.13	0.45	6.42 ± 0.15	6.50 ± 0.15	0.42
TVb (μL)	1.4 ± 0. 2	1.6 ± 0. 2	0.31	1.1 ± 0. 2	1.3 ± 0. 2	0.18
MVb (mL)	0.24 ± 0.05	0.30 ± 0.13	0.37	0.15 ± 0.04	0.19 ± 0.10	0.42
PIF/PEF (mL/s)	0.0111 ± 0.0021	0.0135 ± 0.0067	0.43	0.0078 ± 0.0012	0.0102 ± 0.0032	0.11

Ti: Time of inspiration; Te: time of expiration; f/min: frequency per minute; Phigh: airway pressure high; Pmean: airway pressure mean; TVb: tidal volume; MVb: minute volume; PIF/PEF: peak inspiratory/expiratory flow.

Table S2. 43 proteins involved in supramolecular fiber organization, related to Figure 8.

NO.	Genes	Protein Description	UniProtIds	Fold (5 *Adamts18*$^{-/-}$ /5 *Adamts18*$^{+/+}$)	P Value	AVG Ratio
1	Tmsb10	Thymosin beta-10	Q6ZWY8	0.303	0.029	1.723
2	Rpl13a	60S ribosomal protein L13a	P19253	0.691	<0.001	0.533
3	Fbn2	Fibrillin-2	Q61555	1.401	<0.001	0.486
4	Fbn1	Fibrillin-1	Q61554	1.295	0.001	0.373
5	Pfdn1	Prefoldin 1	Q9CQF7	0.779	0.046	0.360
6	Col1a2	Collagen alpha-2(I) chain	Q01149	1.283	0.037	0.360
7	Col3a1	Collagen alpha-1(III) chain	P08121	1.270	0.018	0.345
8	Tpm3	Tropomyosin alpha-3 chain	D3Z6I8;	0.824	<0.001	0.279
9	Apoe	Apolipoprotein E	P08226	0.825	0.021	0.278
10	Dpysl3	Dihydropyrimidinase-related protein 3	E9PWE8	1.195	0.049	0.257
11	Apoa1	Apolipoprotein A-I	Q00623	0.837	0.009	0.257
12	Arpc3	Actin-related protein 2/3 complex subunit 3	Q9JM76	0.863	0.013	0.213
13	Clu	Clusterin	Q06890	1.150	0.024	0.202
14	Rpl4	39S ribosomal protein L41, mitochondrial	Q9CQN7	1.128	<0.001	0.174
15	Lars	Leucine-tRNA ligase, cytoplasmic	Q8BMJ2	0.890	0.046	0.168
16	Arl2	ADP-ribosylation factor-like protein 2	Q9D0J4	0.891	0.027	0.167
17	Hist1h1b	Histone H1.5	P43276	0.894	0.001	0.162
18	Serpinf2	Alpha-2-antiplasmin	Q61247	0.909	0.034	0.138
19	Vim	Vimentin	P20152	0.916	0.017	0.127
20	Dync1h1	Cytoplasmic dynein 1 heavy chain 1	Q9JHU4	0.918	0.022	0.123
21	Apoa4	Apolipoprotein A-IV	P06728	0.924	0.029	0.114
22	Psmc4	26S proteasome regulatory subunit 6B	P54775	0.925	0.019	0.112
23	Hsp90ab1	Heat shock protein HSP 90-beta	P11499	0.932	0.024	0.102
24	Sptan1	Spectrin alpha chain, non-erythrocytic 1	P16546	0.933	0.002	0.100
25	Rdx	Radixin	P26043	0.934	0.012	0.099
26	Krt8	Keratin, type II	P11679	0.938	0.048	0.092

		cytoskeletal 8				
27	Hsp90b1	Endoplasmin	P08113	0.940	0.001	0.089
28	Add1	Alpha-adducin	Q9QYC0	1.057	0.014	0.080
29	Serpinh1	Serpin H1	P19324	0.952	0.001	0.071
30	Actn4	Alpha-actinin-4	P57780	0.953	0.014	0.069
31	Ran	GTP-binding nuclear protein Ran	P62827	0.959	0.020	0.060
32	Farp1	FERM, ARHGEF and pleckstrin domain-containing protein	F8VPU2	0.959	0.027	0.060
33	Myh10	Myosin-10	Q3UH59	0.964	0.017	0.053
34	Atp2a2	Sarcoplasmic/endoplasmic reticulum calcium ATPase 2	O55143	1.035	0.044	0.050
35	Rock2	Rho-associated protein kinase 2	A0A1Y7VMN0	1.034	0.040	0.048
36	Acta2	Actin, aortic smooth muscle	P62737	0.968	0.008	0.047
37	Mapk1	Mitogen-activated protein kinase 1	P63085	0.972	0.044	0.041
38	Hspa8	Heat shock cognate 71 kDa protein	P63017	0.981	0.016	0.028
39	Kif2c	Kinesin-like protein KIF2C	Q922S8	0.984	0.038	0.023
40	Hist1h1d	Histone H1.3	P43277	0.984	0.001	0.023
41	Map1b	Microtubule-associated protein 1B	P14873	1.016	0.013	0.023
42	Sec24b	Sec24-related gene family, member B (S. cerevisiae)	Q80ZX0	0.986	0.05	0.020
43	Arhgef2	Rho guanine nucleotide exchange factor 2	H3BJ40	0.99	0.044	0.014

AVG: Absolute value of Log2

Table S3. Quantification of important ECM proteins involved in branching morphogenesis in E14.5 lungs, related to Figure 6.

UniProtIds	Gene	Protein Description	mRNA		Protein	Subcellular Location
			H* (3 *Adamts18*$^{-/-}$ /2 *Adamts18*$^{+/+}$)	J* (3 *Adamts18*$^{-/-}$ /3 *Adamts18*$^{+/+}$)	MS (5 *Adamts18*$^{-/-}$ /5 *Adamts18*$^{+/+}$)	
P11087	Col1a1	Collagen alpha-1(I) chain	1.01	1.07	1.36	Extracellular matrix
Q01149	Col1a2	Collagen alpha-2(I) chain	0.96	1.14	1.28 (p = 0.037)	Extracellular matrix
P08121	Col3a1	Collagen alpha-1(III) chain	1.01	1.10	1.27 (p = 0.018)	Extracellular matrix
P11276	Fn1	Fibronectin	1.22	1.23	0.93	Extracellular matrix
P19137	Lama1	Laminin subunit alpha-1	1.25 (p = 0.022)	1.36	0.82	Basement membrane
Q61789	Lama3	Laminin subunit alpha-3	1.60 (p = 0.014)	1.64 (p = 0.016)	0.75	Basement membrane
Q61001	Lama5	Laminin subunit alpha-5	1.17	1.53	0.89	Basement membrane
P02469	Lamb1	Laminin subunit beta-1	1.29 (p = 0.008)	1.29 (p = 0.015)	0.97	Basement membrane
P02468	Lamc1	Laminin subunit gamma-1	1.32 (p = 0.042)	1.26	0.98	Basement membrane
Q3V3R4	Itga1	Integrin alpha-1	0.92	1.28	1.09	Membrane
Q62469	Itga2	Integrin alpha-2	1.15	1.19	1.06	Membrane

Q62470	Itga3	Integrin alpha-3	1.12	1.24	0.99	Membrane
P43406	Itgav	Integrin alpha-v	-	0.98	0.99	Membrane
Q61739	Itga6	Integrin alpha-6	0.95	1.37	1.11	Membrane
P09055	Itgb1	Integrin beta-1	-	0.94	0.99	Membrane
A2A863	Itgb4	Integrin beta-4	0.81	1.77	-	Membrane
P18828	Sdc1	Syndecan-1	1.21	-	-	Extracellular matrix
O35988	Sdc4	Syndecan-4	1.10	-	-	Extracellular matrix
Q62165	Dag1	Dystroglycan	1.10	1.28* (P = 0.050)	1.3	Basement membrane
P10493	Nid1	Nidogen-1	1.18	1.27 (P = 0.007)	0.99	Basement membrane
P33434	Mmp2	72 kDa type IV collagenase	0.78	-	0.97	Extracellular matrix
P29268	Ctgf	CCN family member 2	0.92	1.51 (P = 0.036)	-	Extracellular matrix
P04202	Tgfb1	Transforming growth factor beta-1 proprotein	0.84	1.02	-	Extracellular matrix

*H and J represent mice from two different littermates.

"-": mean data unavailable because of limited quantity of samples in real-time *q*PCR experiments or undetectable in MS analysis.

Table S4. Antibodies used in this study, related to Figure 4, 6, 8, S2, and S4.

Name	Catalog number	Company	Application (dilution)
Anti-MYC	TA150121	Origene	ICC (1:100)
Anti-Fibrillin1	Ab53076	Abcam	ICC (1:100)
Anti-DDK	TA150078	Origene	WB (1:5000)
Anti-FBN1-C ternimal	LS-C358981	LifeSpan Bioscience	WB (1:400)
Anti-FBN2	Sc-393968	Santa Cruze	WB (1:200)
Anti-FBN2	20252-1-AP	Proteintech	IHC (1:200)
Anti-FAK	AF6397	Affinity	IHC (1:100)
Anti-PFAK(Tyr397)	AF3398	Affinity	IHC (1:100)
Anti-TMSB10	TA351779	Origene	IHC (1:50)
Anti-Fgf10	GTX55619	Genetex	IHC (1:100)
Anti-Fgfr2	23328	CST	IHC (1:200)
Anti-CD11b	Ab133357	Abcam	IHC (1:2000)
Anti-MPO	AF3667	R&D system	IHC (1:40)
Anti-Histone H3	NB100-57135	Novus	IHC (1:200)
CY^{TM}3 Affinity Goat Anti-Rat IgG	112-165-003	Jackson Immuno Research	IHC/ICC (1:200)
CY^{TM}3 Affinity Goat Anti-Rabbit IgG	111-165-003	Jackson Immuno Research	IHC/ICC (1:200)
Alexa Fluor 488 Donkey Anti-Rabbit IgG	705-545-147	Jackson Immuno Research	IHC (1:200)
Alexa Fluor 647 Donkey Anti-Goat IgG	711-605-152	Jackson Immuno Research	IHC (1:200)

Table S5. Primers for quantitative real-time RT-PCR (*q*RT-PCR), related to Figure 1, 4, 5, 6, S1, S2, and S5.

Gene	Forward (5' to 3')	Reverse (5' to 3')
Gapdh	*GTGGAGTCATACTGGAACATGTAG*	*AATGGTGAAGGTCGGTGTG*
Adamts18	CCTCAAGTTGTCTGCTCCATCA	GCTGAAGAAATCCACGCAAGA
Fbn1	GCCAGAAAGGGTACATCGG	ACACACCTCCCTCCGTT
Fbn2	GTGAAACCACACAGAAATGTGAA	GAACAGTCGCCAGTCTCAC
Eln	CTGCTGCTAAGGCTGCTAAG	CCACCAACACCAGGAATGC
Lox	TCTTCTGCTGCGTGACAACC	GAGAAACCAGCTTGGAACCAG
Fbln4	CTCTGGGCGTTTCTGCTGTT	GCCATCTGTGCATTCCGTGT
Fbln5	GGGCTCATACTTCTGCTCG	GATGGTGAATGGCTGGTCT
Tgfb1	CTCCCGTGGCTTCTAGTGC	GCCTTAGTTTGGACAGGATCTG
Ltbp1	GGTTATTTGCCATCTTCCGTGTA	GAAATTTGGAGGGCACTGACA
Itgav	GGCACAAAGACCGTTGAGTA	ACCAGGACCACCGAGAAGTA
Itgb3	AGGGCAGTCCTCTATGTGGT	CTTGGCTCTGGCTCGTTCT
Mmp2	GACCATGCGGAAGCCAAGA	TGTGTAACCAATGATCCTGTATGTG
Mmp12	CACAGGAGGAACTATGAGTAGCA	AGGCAGACCAGGACACAGA
Col1a1	CGGTGCTACTGGAGTTCAAGGT	CAGGGAAACCACGGCTACCA
Col3a1	CCACAAGGATTACAAGGCATACC	TCCAGGAGCACCGACTTCA
Col4a1	AATGGCATTGTGGAGTGTCAAC	TTCTGTCCAACTTCACCTGTCAA
Fgf10	TCCGTACAGTGTCCTGGAGATA	CCCTTCTTGTTCATGGCTAAGTAAT
Fgfr2	CGCTTCATCTGCCTGGTCTTG	ACGGTGCTCCTTCTGGTTCTAA
Wnt2	CCTGATGAACCTTCACAACAACA	GCCACTCACACCATGACACT
Bmp4	AGCCCGCTTCTGCAGGA	AAAGGCTCAGAGAAGCTGCG
Shh	CTCCGAACGATTTAAGGAACTCAC	GCCACTGGTTCATCACAGAGAT
Hhip	GGAGCCTTACTTGGACATTCAC	CCGTTCCTGGTTGGTGGTAT
Ptch1	CTCAGGCAATACGAAGCACAG	GGAGGCTGATGTCTGGAGTC
Ext1	GTTGCCATTCTCCGAAGTGATT	TGTGTCTGCTGTCTAAGTGCTA
Col1a2	CGATGTTGAACTTGTTGCTGAG	GGCAGGCGAGATGGCTTAT
Fn1	AAGAGAAGACAGGACCAATGAA	TTGAGAGCATAGACACTGACTT
Lama1	GCTATCCTGCCCACATCAAAC	CAAGGACTGCACTTGTGAGC
Lama3	CTCCAATGACCTCAGTCCAGAA	TCTCAGAACGATGCGGAACA
Lama5	TTGGAGAATGGCGAGATTGTG	CGAAGTAACGGTGAGTAGGAGA
Lamb1	TCTGTGAACCATGTACCTGTGA	GACACTGACCAGCAATGAGAC
Lamc1	TGCCGCCAATGTGTCAATC	TGCCACTCGTACAATGTCATC
Sdc1	CTGGAGAACAAGACTTCACCTT	AGCACTTCCTTCCTGTCCAA
Sdc4	ACCTCCTGGAAGGCAGATACT	GGCACCAAGGGCTCAATCA
Dag1	GAGTGAGCATTCCAACGGATT	CAGTGTAGCCAAGACGGTAAG
Ctgf	AAGGACCGCACAGCAGTT	AGTTGGCTCGCATCATAGTTG
Nid1	AGAGCAACGGAGCCTATAACAT	CGGTAGCAGGACTTCCAATCT
Itga1	CGGCTTCAGTGCTCATTATTCA	ATGACCACAGTTCCGTTCCA
Itga2	CGCAAGAGACTACGCTTATTCA	CTCGCCATCGGTCACAACT
Itga3	AGAGACACATTGCCAGACACT	CGCAGAGGTAAGGAGTAGTTCA

Itga6	TCTCGTTCTTCGTTCCAGGTT	GCAGCAGCGGTGACATCTA
Itgb1	TGGTCAGCAACGCATATCTG	GTTACATTCCTCCAGCCAATCA
Itgb4	GACCAATGGCGAGATCACAG	TCCACGAGCACCTTCTTCATA
Snail1	GTCTGCACGACCTGTGGAAA	GGTCAGCAAAAGCACGGTTG
Snail2	TCATCCTTGGGGCGTGTAAG	GATGGCATGGGGGTCTGAAA
Cdh1	CAGCCGGTCTTTGAGGGATT	TGACGATGGTGTAGGCGATG
Cdh2	ACAGCGCAGTCTTACCGAAG	CTTGAAATCTGCTGGCTCGC
Vim	TTCTCTGGCACGTCTTGACC	GCTTGGAAACGTCCACATCG

Transparent Methods

Reagents

All reagents were purchased from Sigma–Aldrich (St. Louis, MO, USA) unless otherwise indicated. Primary antibodies used in this study are listed in Table S4.

Animals

Adamts18 knockout (*Adamts18*$^{-/-}$) and wildtype (*Adamts18*$^{+/+}$) mice with the C57BL/6/129Sv background were generated and genotyped as previously described (Lu et al., 2017). Animals were maintained on a 12-h light/dark schedule (lights on at 06:00) in a specific pathogen-free facility. All procedures for animal experiments were approved by the Institutional Animal Care and Use Committee of East China Normal University (ECNU).

RNA in situ hybridization

RNA in situ hybridization (ISH) was performed as described previously (Zhu et al., 2019). Briefly, mouse lungs were fixed in 10% neutral buffered formalin for 24 h at room temperature (RT) and paraffin-embedded following standard methods. ISH was performed on 5-μm-thick sections using the RNAscope 2.5 HD Reagent Kit-RED (Advanced Cell Diagnostics, Hayward, CA). Specific probes were used to detect target mRNAs as described (Zhu et al., 2019).

Quantitative Real-Time RT-PCR Analysis

Quantitative real-time RT-PCR (*q*RT-PCR) was performed using the Step One Plus real-time PCR system (ThermoFisher, Carlsbad, CA) with SuperReal PreMix Plus (SYBR Green; TIANGEN). Primers used are listed in Table S5. The relative quantity of target mRNA was determined using the *ΔΔCt* method, with *Gapdh* as the reference gene. All reactions were performed in triplicates.

Explant cultures

Lung explant cultures were performed as previously described (Moral and Warburton, 2009). Briefly, E11.5 lungs were cultured on Nucleopore polycarbonate track-etch membranes (WHA-110414, Whatman) at 37°C in a 5% CO_2 incubator for 72 h. For the rescue experiments, sense and antisense-phosphorothioated oligodeoxynucleotides (SODN and ASODN) were synthesized and added to the culture medium at the concentration of 0.5 μM for *Fbn1* or 1 μM for *Fbn2 (Kanwar et al., 1998; Yang et al., 1999)*. Sequences of the oligonucleotides are as follows: *Fbn1* sense ODN: 5'-GCCAGCGCGACCTCCAGCAGCCCTCCTCGCCGCAT-3', *Fbn1* aitisense ODN: 5'-ATGCGGCGAGGAGGGCTGCTGGAGGTCGCGCTGGC-3', *Fbn2* sense ODN: 5'-CTCGGAGTATTTCCTGCTGTCCTCGCCTGCGGAC-3', *Fbn2* antisense ODN: 5'-GTCCGCAGGCGAGGACAGCAGGAAATACTCCGAG-3'. The culture medium was refreshed every 24 h. Images of explants were taken using an Mshot microscope with MS60 camera (Guangzhou, China). The number of branches was counted manually, and the length of each airway was calculated by the software Image Pro

Plus 6.0 (IPP, Media Cybernetics, Inc., Silver Spring, MD, USA).

Lung cast

Mice were euthanized by CO_2 asphyxiation. The trachea was exposed just below the larynx, and a catheter was inserted and securely tied with braided silk surgical suture. The lungs were inflated with casting agent (90 ml ethyl acetate, 10 g polyvinyl chloride, 2.7 ml dibutyl phthalate, and appropriate amount of oil paints), separated from trachea, and transferred to a 60°C oven. After the casting agent was solidified, the lungs were immersed in 50% HCl to remove tissues (only airways left). Airways were imaged using an Mshot microscope.

Histology, immunohistochemistry, and immunofluorescence

Lung tissues were fixed in 10% neutral buffered formalin and embedded in paraffin. After dewaxing and rehydration, hematoxylin and eosin (HE) staining or Hart's staining was performed on 5-μm sections to determine radial alveolar counts (RAC) and elastin distribution. Immunohistochemical staining of sections was performed using anti-CD11b, anti-histone H3, anti-MPO, anti-FBN1, anti-FBN2, anti-PFAK (Tyr397), anti-FAK, anti-TMSB10, anti-FGF10, and anti-FGFR2 antibodies. For immunofluorescence examination, 48 h after transfection, the cells were fixed with pre-cooled ethanol for 20 min. The samples were incubated with anti-ddk (or anti-myc), anti-fibrillin1, and anti-fibrillin2 antibodies overnight at 4°C, followed by incubation with the secondary antibody. Samples were counterstained with DAPI (MP, Carlsbad, CA) and imaged with a Leica SP8 confocol microscope (Leica Microsystems, Wetzlar, Germany).

FITC-phalliodin staining

E14.5 lung tissues were obtained, embedded in optimal cutting temperature (OCT) compound, and cut into 10-μm thick sections with a Leica CM3050 S cryostat microtome (Leica Biosystem, Wetzlar, Germany). The sections were fixed for 15 min with 4% formaldehyde in PBS and permeabilized with 0.5% triton X-100 in PBS for 20 min, followed by incubation with 0.1 mg/ml FITC-phalloidin diluted in PBS containing 1% BSA at 37°C for 2 h and counterstaining with DAPI. After mounting on slides, the sections were examined with a Leica SP8 confocal microscope.

Lung function examination

Mice were anesthetized with a mixture of urethane (14% m/v), alpha-chloralose (0.7% m/v), and sodium tetraborate decahydrate (0.7% m/v) in saline and connected to a computer-controlled ventilator via the tracheal cannula. After normal respiratory movements were recorded, mice were mechanically ventilated with room air at 110 breaths per min with the expiration/inspiration ratio of 20:10. Pulmonary function tests were performed using the AniRes2005 Lung Function System (Bestlab Technology Co., Ltd).

LPS-induced acute lung injury

Lipopolysaccharide (LPS) was diluted to a final concentration of 1 mg/ml in normal saline. Anesthetized mice were injected intraperitoneally (I.P.) with LPS at 10 mg/kg. Lung tissues were collected at different time points (0 h, 3 h, 6 h, 12 h, and 24 h) after LPS injection. Pathological grade of lung injury was defined as follows: Grade 0, normal alveoli, alveolar septum, and bronchi; Grade 1, partial alveolar septal congestion; Grade 2, moderate alveolar septal congestion and intra-alveolar hemorrhage; Grade 3, severe congestion and bleeding in alveolar septum and alveoli. Frozen lung tissues (around 30 mg) were homogenized to measure IL-6 using a commercially available ELISA kits (LYBD Bio-Technique Co, Ltd, Beijing, China), and data were normalized to protein concentration measured by the bicinchoninic acid (BCA) method.

Bronchoalveolar lavage

Mice were sacrificed by CO_2 asphyxiation and bronchoalveolar lavaged 3 times, each with 0.8 ml of PBS via a 22G catheter. The bronchoalveolar lavage fluid (BALF) was centrifuged at 400 xg for 7 min at 4°C, and the pellet was resuspended in 20 µl PBS containing 1% BSA. The resuspended cells were placed on a slide, dried, stained with Diff-Quick (Solarbio Life Science, Beijing, China), and counted under a microscope at 100x magnification.

Bleomycin-induced lung fibrosis

Mice were anesthetized and intratracheally instilled with 100 µl of saline or bleomycin sulfate dissolved in saline (1 mg/kg body weight), followed with 300 µl of air to ensure delivery to the distal airways. Mouse mortality was monitored for 25 days after bleomycin injection. To assess lung fibrosis, mice were sacrificed, and lung tissues were examined microscopically at 100 x magnification. The severity of fibrosis was determined according to the method of Ashcroft et al (Ashcroft et al., 1988) and scored as follows: grade 0, normal lung; grade 1, minimal fibrous thickening of alveolar or bronchiolar walls; grade 3, moderate thickening of walls without obvious damage to lung architecture; grade 5, increased fibrosis with definite damage to lung structure and formation of fibrous bands or small fibrous masses; grade 7, severe distortion of structure and large fibrous areas; grade 8, total fibrous obliteration.

Proteomic analysis of embryonic lungs

Whole lung tissues from E14.5 embryos were digested with sequencing grade trypsin (Promega) and fractionated with high PH reversed phase chromatography. The data-independent acquisition (DIA) analysis was performed on an Orbitrap Fusion LUMOS mass spectrometer (Thermo Fisher Scientific) connected to an Easy-nLC 1200 via an Easy Spray (Thermo Fisher Scientific). The DIA raw files were analyzed in Spectronaut X (Biognosys, Schlieren, Switzerland). Pathway enrichment analysis was performed with MetaScape (http:// metascape.org/).

Transmission electron microscopy (TEM)
Distal parts of E14.5 lungs were fixed with 2.5% glutaraldehyde at 4°C, followed by fixation with osmium tetroxide, dehydration in alcohol, embedding in plastic, ultra-thin sectioning, flotation of the sections on aqueous medium, and staining with uranyl acetate and lead acetate. Images were taken with a Tecnai G2 Spirit BioTWIN transmission electron microscope (FEI, Hillsboro, Oregon).

ADAMTS18 and fibrillin1 (FBN1) expression
The plasmid for expression of Myc-DDK tagged mouse full-length *Adamts18* (pCMV6-*Adamts18*, the ORF clone with sequence NM_172466 in pCMV6-Entry) was purchased from Origene (Rockville, MD). Plasmid DNA was introduced into HEK293T cells by transfection using Lipofectamine 2000 (Invitrogen/Life technologies, Carlsbad, CA).

Co-Immunoprecipitation (IP)
Mouse dermal fibroblast cells (DFCs) and HEK293T cells were co-cultured and transiently transfected with pCMV6-*Adamts18* or empty vector. At 48 h, the cells were washed once with PBS and lysed in NP-40 buffer (50 mM Tris-base pH 7.5, 150 mM NaCl, 1% NP-400, and protease inhibitors). Cell lysates were incubated with anti-DDK agarose (TA150037, Origene, Rockville, MD) at 4°C overnight and washed with 1% NP40 washing buffer. The proteins eluted from the agarose beads were resolved by SDS-PAGE and analyzed by Western blotting with anti-fibrillin 1 C-terminal, anti-fibrillin 2, and anti-DDK (DYKDDDDK) primary antibodies and horseradish peroxidase (HRP)-conjugated secondary antibody. The immunoreactive bands were visualized with enhanced chemiluminescence (ECL) Western blot kit (Millipore, Boston, MA).

RhoA Activity
RhoA activity was detected using the Rho Activation Assay Biochem Kit (Cytoskeleton, Inc, Dencer, CO). Briefly, E15.5 lung tissues were isolated and homogenized in the lysis buffer. The cell lysate thus obtained was adjusted to 1 mg/ml of protein and then incubated with rhotekin-RBD beads at 4°C for 1 h. RhoA was then eluted from the rhotekin-RBD beads and analyzed by Western blotting with anti-RhoA antibody included in the kit.

Statistics
Data were analyzed by Student's *t* test or Log-rank (Mantel-Cox) test using the software package Prism version 7 (GraphPad, La Jolla, CA, USA). Data are shown as mean ± SEM or mean ± SD. A p value < 0.05 was considered statistically significant.

Supplemental Reference
Ashcroft, T., Simpson, J.M., and Timbrell, V. (1988). Simple method of estimating severity of pulmonary fibrosis on a numerical scale. Journal of clinical pathology *41*, 467-470.

Kanwar, Y.S., Ota, K., Yang, Q., Kumar, A., Wada, J., Kashihara, N., and Peterson, D.R. (1998). Isolation of rat fibrillin-1 cDNA and its relevance in metanephric development. The American journal of physiology *275*, F710-723.
Lu, T., Dang, S., Zhu, R., Wang, Y., Nie, Z., Hong, T., and Zhang, W. (2017). Adamts18 deficiency promotes colon carcinogenesis by enhancing beta-catenin and p38MAPK/ERK1/2 signaling in the mouse model of AOM/DSS-induced colitis-associated colorectal cancer. Oncotarget *8*, 18979-18990.
Mei, S.H., McCarter, S.D., Deng, Y., Parker, C.H., Liles, W.C., and Stewart, D.J. (2007). Prevention of LPS-induced acute lung injury in mice by mesenchymal stem cells overexpressing angiopoietin 1. PLoS medicine *4*, e269.
Moral, P.M.D., and Warburton, D. (2009). Explant culture of mouse embryonic whole lung, isolated epithelium, or mesenchyme under chemically defined conditions as a system to evaluate the molecular mechanism of branching morphogenesis and cellular differentiation. Methods Mol Biol *633*, 71-79.
Yang, Q., Ota, K., Tian, Y., Kumar, A., Wada, J., Kashihara, N., Wallner, E., and Kanwar, Y.S. (1999). Cloning of rat fibrillin-2 cDNA and its role in branching morphogenesis of embryonic lung. Dev Biol *212*, 229-242.
Zhu, R., Pan, Y.H., Sun, L., Zhang, T., Wang, C., Ye, S., Yang, N., Lu, T., Wisniewski, T., Dang, S.*, et al.* (2019). ADAMTS18 Deficiency Affects Neuronal Morphogenesis and Reduces the Levels of Depression-like Behaviors in Mice. Neuroscience *399*, 53-64.